Few-Outcome Readout of Quantum-Fisher-Optimal Measurements: Sharp Bounds and Coherent-Synthesis Hardness

Maestro v0.1
Pudim AI

August 20, 2026

Abstract

A quantum-Fisher-optimal measurement may resolve exponentially many eigenvectors even when its information-bearing score needs only a small outcome alphabet. We quantify this separation. For any partition of the symmetric-logarithmic-derivative (SLD) spectrum, the lost quantum Fisher information is the state-weighted within-bin score variance. We derive a sharp $\delta^2/4$ resolution law, a dimension-free tail theorem, and a Wasserstein-controlled dense-spectrum crossover. In a frustrated four-spin sensor, the best product measurement found by the archived heuristic search retains 48.55% of F_Q, while eight globally optimized contiguous score bins retain 99.26%. For coherent compilation, we separate an approximate SLD block encoding from the implemented label circuit and prove an operational interface: a uniform score-intertwining defect controls both the actual POVM's Fisher loss and the reconstructed signal operator. A full-support embedding then establishes BQP-hardness for coherent compilers satisfying this interface at inverse-polynomial accuracy; achieving the interface with the quoted primitive cost remains conditional on the underlying spectral-processing guarantee. A parity-coherence sensor has constant conditioning, extensive F_Q, and only $n+1$ scores. The results form a rigorous readout, certification, and compilation toolkit without asserting an end-to-end laboratory advantage.

1 Introduction

The quantum Fisher information (QFI) is usually presented as a scalar optimum over measurements. A metrological device needs more: it must realize a measurement that extracts that information from new state copies. For a one-parameter model, the canonical optimum is the spectral measurement of the symmetric logarithmic derivative (SLD) [1, 2, 3, 4, 5]. On an n-qubit mixed state, that observable can be dense and can have 2^n eigenvectors. This creates two separate questions: how many distinct *scores* must a detector resolve, and how hard is it to compile the projectors carrying those scores?

This paper leads with the first question. The outcome of an SLD measurement is useful only through its local score, so degeneracies and nearby scores should be compressible. We identify coarse SLD readout with scalar quantization of the state-weighted score spectrum and derive sharp detector guarantees: a tight finite-resolution coefficient, a dimension-free tail construction, Wasserstein stability from finite spectra to a dense-spectrum limit, and the exact finite-support crossover. The foundational conditional-variance identity has a broader contemporaneous antecedent in task-dependent syndrome compression; Sec. 10 gives the precise priority boundary. The results claimed here begin with the sharp lossy detector bounds and their integration with physical measurement synthesis.

The second question has direct-search and coherent-algorithmic forms. In the direct branch, one may search over a declared family of experimentally realizable projective measurements. We derive an exact completion-of-the-square certificate for the resulting Fisher loss and then invoke the general benign projective-landscape theorem of Ref. [6]: projective local maxima and second-order stationary points are globally optimal, while every nonglobal critical point has an explicit two-vector escape. This exact geometry does not by itself supply a dimension-independent convergence rate or robustness to ansatz restriction and sampling noise. At the coherent layer, one may solve the SLD Lyapunov equation in block-encoded form and process an approximate score operator. We formulate a uniform score-intertwining interface between that matrix approximation and the actual implemented label POVM. The common object is the score operator L, and the exact Fisher-loss identity connects both regimes.

The computational setting is motivated by a current tension in quantum algorithms. Structure that removes barren plateaus can also expose efficient classical simulation, whereas an abstract BQP-hard primitive can lose that status after physical restrictions are imposed [7, 8, 9, 10, 11, 12, 13]. Here the restrictions are stringent: positivity, trace normalization, faithfulness, controlled conditioning, finite spectral resolution, and a uniform coherent output contract. We embed positive quantum linear systems into an SLD with *full spectral support*; the QLS information occupies eigenvectors throughout the score spectrum. The marginal score histogram is independent of the linear-system right-hand side, while coherent signal reconstruction recovers it. The synthesis task satisfying the declared interface remains BQP-hard. Section 2 separates this coherent output problem from ordinary sampling on the sensor state.

Quantum metrology supplies the physical context. The QFI governs local sensing, interferometry, spectroscopy, and many-body metrology [14, 15, 16, 17, 18, 19, 20, 21]. QFI estimation, randomized measurements, shadows, Krylov hierarchies, incomplete-data witnesses, and variational protocols address the value problem without generally compiling its optimal measurement [22, 23, 24, 25, 26, 27, 28, 29, 30, 31, 32]. Structured SLD constructions exploit exponential families, anticommutator closure, tensor networks, Gaussianity, master equations, or symmetry [33, 34, 35, 36, 37, 38, 39, 40, 41]. Coarse detectors can preserve quantum enhancement in specific experiments [42]; the theorems below give a model-independent score-space account of that phenomenon.

The coherent linear-algebra primitive is a Sylvester equation. Classical Sylvester and Lyapunov solvers are mature [43, 44]. Somma, Low, Berry, and Babbush (SLBB) construct a block encoding of the solution of $AX + XB = C$ and show that the general primitive can encode BQP-complete computation [45]. Block encoding differs from the ℓ^2 sample-and-query access used by quantum-inspired low-rank algorithms [46, 47, 48, 49]. We make that access-model distinction explicit and identify which special instances remain dequantizable.

1.1 Notation and result map

At a fixed SLD-regular operating point, write ρ for the state and $\dot\rho$ for its derivative. Let L be the canonical SLD,

$$\rho L + L\rho = 2\dot\rho, \qquad F_Q := \mathrm{Tr}(\rho L^2). \tag{1}$$

For a rank-one PVM $P = (P_j)$ with occupied outcome probabilities

$$q_j := \mathrm{Tr}(\rho P_j), \qquad r_j := \mathrm{Tr}(\dot\rho P_j), \tag{2}$$

define

$$\ell_j := r_j/q_j, \quad J(P) := \sum_{j:q_j>0} \frac{r_j^2}{q_j}, \quad L_P := \sum_{j:q_j>0} \ell_j P_j. \tag{3}$$

The state-weighted SLD score measure is

$$\nu_{\rho,L}(\Omega) := \mathrm{Tr}[\rho\,\mathbf{1}_\Omega(L)]. \tag{4}$$

For a spectral partition $\mathcal{I} = (I_b)_b$, $J_{\mathcal{I}}$ denotes the Fisher information of $B_b = \mathbf{1}_{I_b}(L)$. We write J_δ when every occupied bin has diameter at most δ, and $J_K^\star$ for the best contiguous partition with at most K bins. The optimal scalar squared-error distortion of a probability measure ν is

$$D_K(\nu) := \inf_{|C|\le K} \int \mathrm{dist}(\lambda, C)^2\,\nu(\mathrm{d}\lambda). \tag{5}$$

When $\mu I \preceq S \preceq \Lambda I$, $\kappa := \Lambda/\mu$. For an SLD with no zero score, define its *zero-score margin*

$$g_0(L) := \min\{|\lambda| : \lambda \in \mathrm{spec}(L)\}. \tag{6}$$

This is the distance of the score spectrum from zero, not the minimum spacing between distinct scores. The coherent input model supplies block encodings of a common scaling $S = c\rho$ and $D = c\dot\rho$; it does not assume classical sample-and-query access to their entries.

Our contributions are:

R1 Sharp few-outcome readout. We use the exact score-projection identity

$$F_Q - J_{\mathcal{I}} = \sum_b q_b \,\mathrm{Var}(\lambda \mid I_b) \tag{7}$$

to prove the sharp arbitrary-bin bound

$$F_Q - J_{\mathcal{I}} \le \frac{1}{4}\sum_b q_b\,\mathrm{diam}(I_b)^2, \qquad F_Q - J_\delta \le \frac{\delta^2}{4}, \tag{8}$$

and the dimension-free tail construction

$$F_Q - J_{K+2} \le T_R + \frac{R^2}{K^2}, \qquad T_R := \int_{|\lambda|>R} \lambda^2 \nu_{\rho,L}(\mathrm{d}\lambda). \tag{9}$$

We further prove Wasserstein stability and a dense-spectrum high-rate window with the exact finite-atomic crossover. These are the main readout results.

R2 Projective-search certificate. We derive inline the exact residual identity

$$F_Q - J(P) = \mathrm{Tr}[\rho(L_P - L)^2]. \tag{10}$$

The companion Landscape theorem [6] then supplies the nonconvex geometry: every projective local maximum and second-order stationary point is globally POVM-optimal, and every nonglobal critical PVM has an explicit pair-rotation escape. Equation (10) is an exact stopping certificate for experimental or variational search.

R3 Operational compiler interface and full-support hardness. We separate the Hermitian matrix approximation from the actual label circuit. A uniform score-intertwining defect bounds both the implemented POVM's Fisher loss and the reconstructed signal operator. A faithful, trace-normalized embedding with full score support, polynomial conditioning, an inverse-polynomial zero-score margin, and inverse-polynomial QFI proves BQP-hardness for coherent compilers satisfying this interface at inverse-polynomial accuracy. The hard information resides in the SLD eigenvectors; the marginal score histogram is independent of the encoded right-hand side. Primitive-level quantum-polynomial implementation cost remains conditional on certifying the interface.

R4 Promise-compatible sensing and audited numerics. We exhibit an n-qubit parity-coherence sensor with constant $\kappa = 3$, extensive $F_Q = n/4$, and only $n+1$ exact SLD scores. For Gibbs access we prove the rescaling-invariant obstruction $\kappa = e^{\beta \Delta E_n}$ and report a finite-size shrinking-temperature study through ten spins without promoting its leading-order sample scaling to a theorem. In a frustrated four-spin benchmark, the best product PVM found by the archived heuristic search retains 48.55% of F_Q, whereas globally optimized contiguous seven- and eight-bin score readouts retain 98.34% and 99.26%. Deterministic executable gates validate the archived identities and finite-dimensional reductions.

Result R1 applies to faithful, pure, and rank-deficient models at SLD-regular operating points and requires no condition-number promise. Faithfulness is needed only for the smooth global projective-landscape theorem, the conditioned Sylvester bounds, and the present hardness construction. Section 2 states the exact support condition.

Section 3 proves R1. Section 4 derives Eq. (10) and imports only the geometric theorems needed for R2. Sections 5 and 6 give the conditioning diagnostic and coherent compiler. Section 7 proves R3. Sections 8 and 9 establish R4. Sections 10 and 11 delimit prior work, dequantization, and scope.

2 Local metrology, support, and access models

This section separates the assumptions needed for finite-outcome readout, projective landscape geometry, and coherent compilation. The distinction is important: pure and rank-deficient probes are covered by Result R1 at regular operating points, even though a coefficient-conditioned Sylvester solver necessarily requires a faithful state.

2.1 Canonical SLD and the support-regularity condition

Let ρ_θ be a differentiable density-operator family on a d-dimensional Hilbert space, with $d = 2^n$ in an n-qubit implementation. At the operating point write $\rho = \rho_\theta \geq 0$, $\dot{\rho} = \partial_\theta \rho_\theta$, and let

$$\Pi_0 := \mathbf{1}_{\{0\}}(\rho) \tag{11}$$

project onto the kernel of ρ. We call the operating point *SLD regular* when

$$\boxed{\Pi_0 \dot{\rho} \Pi_0 = 0.} \tag{12}$$

In finite dimension, Eq. (12) is necessary and sufficient for a bounded Hermitian solution of the global Lyapunov equation $\rho L + L\rho = 2\dot{\rho}$. It holds automatically for a two-sided differentiable path through the positive cone: every quadratic form supported in $\ker \rho$ has a local minimum at the operating point. It includes ordinary pure-state and fixed-rank models. It can fail at one-sided rank-changing boundaries, where the SLD may become unbounded and the pointwise QFI requires a limiting treatment [50, 51, 52, 53].

In an eigenbasis $\rho = \sum_i p_i |i\rangle\langle i|$, the canonical bounded SLD at an SLD-regular point is

$$L = 2 \sum_{i,j : p_i + p_j > 0} \frac{\langle i|\dot{\rho}|j\rangle}{p_i + p_j} |i\rangle\langle j|, \tag{13}$$

with its arbitrary joint-kernel action fixed to zero. It obeys the operator identity

$$\rho L + L\rho = 2\dot{\rho} \tag{14}$$

on the full Hilbert space, and the SLD QFI is

$$F_Q = \mathrm{Tr}(\rho L^2) = \mathrm{Tr}(\dot{\rho} L) < \infty. \tag{15}$$

For example, a differentiable pure-state path obeys Eq. (12), has $L = 2\dot{\rho}$ on the relevant two-dimensional tangent support, and is covered by the readout results below. By contrast, $\rho_\theta = (1-\theta)|0\rangle\langle 0| + \theta |1\rangle\langle 1|$ at the one-sided endpoint $\theta = 0$ violates Eq. (12) and lies outside the pointwise theorem.

A rank-one PVM $P = (P_j)$ gives

$$q_j = \mathrm{Tr}(\rho P_j), \qquad r_j = \mathrm{Tr}(\dot{\rho} P_j). \tag{16}$$

Only occupied outcomes contribute, and the omission of zero-probability outcomes is exact rather than conventional. Indeed, for a rank-one outcome $P_j = |j\rangle\langle j|$, positivity gives

$$q_j = 0 \implies |j\rangle \in \ker \rho. \tag{17}$$

SLD regularity then implies

$$r_j = \langle j|\dot{\rho}|j\rangle = \langle j|\Pi_0 \dot{\rho} \Pi_0|j\rangle = 0. \tag{18}$$

Thus

$$\ell_j = \frac{r_j}{q_j}, \qquad J(P) = \sum_{j : q_j > 0} \frac{r_j^2}{q_j}, \qquad L_P = \sum_{j : q_j > 0} \ell_j P_j, \tag{19}$$

with no information discarded by the restricted sums. The Braunstein–Caves inequality is $J(P) \leq F_Q$, with equality for a sufficiently refined SLD eigenbasis [3, 4].

For a spectral partition $(I_b)_b$ of L, let

$$B_b = \mathbf{1}_{I_b}(L), \qquad \sum_b B_b = I. \tag{20}$$

The state-weighted measure $\nu_{\rho,L}$ assigns zero mass to arbitrary kernel components of L, so all score-compression statements are independent of the joint-kernel convention. Result R1 therefore applies to pure states, GHZ probes, squeezed states, and low-rank models whenever Eq. (12) holds.

2.2 Three output notions and an operational circuit interface

A scalar QFI estimate, a state proportional to a Lyapunov solution, and a coherent observable are different computational outputs. The circuit-level object used here is the parameter-independent isometry

$$V : \mathcal{H} \longrightarrow \mathcal{H} \otimes \mathcal{K} \tag{21}$$

induced by the actual implemented unitary on initialized ancillas at the fixed operating point. Let $(P_y)_y$ be exhaustive orthogonal projectors on the output-label space, including every ordinary, boundary, leakage, and failure label. The measured operation is the POVM

$$M_y = V^\dagger P_y V, \qquad \sum_y M_y = I. \tag{22}$$

Every label has a declared bounded numerical score c_y, collected in

$$C = \sum_y c_y P_y. \tag{23}$$

For a Hermitian matrix-layer approximation $\widetilde{L}$, the operational error is the uniform score-intertwining defect

$$\xi = \|CV - V\widetilde{L}\|_\infty. \tag{24}$$

This contract charges binning, boundary behavior, leakage, and failure through their assigned scores. Measuring the label register implements the actual POVM (M_y); it need not equal an exact coarse SLD PVM. Retaining the label coherently permits spectral transformations and supplies the output used in the hardness reduction. A block encoding of L supports qubitization, Hamiltonian simulation, and coherent filtering; a prepared mixed state proportional to L alone does not supply those operations [54, 55, 56, 57, 58, 45].

For local estimation, a preliminary estimator can locate the operating point using a vanishing sample fraction; the SLD measurement at that estimate is then applied to the remaining copies [4, 59, 60]. We study the computational subroutine at the fixed operating point.

2.3 Where faithfulness enters

The principal claims require different regularity:

- The exact spectral-compression identity and its sharp consequences require Eq. (12) and finite F_Q, but no lower eigenvalue bound or condition number.
- The smooth global projective-landscape theorem imported from Ref. [6] is currently stated for $\rho > 0$, so Result R2 uses faithfulness. Extending its critical-point classification to probability strata is separate from the compression theorem.
- The conditioned coherent compiler assumes a strictly positive lower spectral bound. Its κ-dependent error bounds become uninformative as $\mu \to 0$; they are not claims about generic pure-state compilation.

These assumptions are carried explicitly through the result map rather than deferred to the discussion.

2.4 Balanced block-encoding promise

For coherent compilation we therefore assume $\rho > 0$. Density matrices have trace one, so their raw eigenvalue scale can be exponentially small. Use a common physical scaling

$$S = c\rho, \qquad D = c\dot{\rho}, \qquad SL + LS = 2D, \tag{25}$$

which leaves the SLD invariant.

Assumption 2.1 (Promised input model)**.** *The input provides efficient block encodings of S/Λ and $D/(\alpha\Lambda)$ such that*

$$0 < \mu I \preceq S \preceq \Lambda I, \qquad \kappa = \Lambda/\mu = \mathrm{poly}(n), \\ \alpha = \mathrm{poly}(n), \tag{26}$$

and provides the positive square-root access required by the accelerated Sylvester routine of Ref. [45]. The matrix error $\eta = \|\widetilde{L} - L\|_\infty$, score-intertwining defect ξ, and any controlled-signal error are requested at inverse-polynomial accuracy. A primitive-level query bound is used only when the corresponding spectral-processing routine certifies these uniform quantities.

Assumption 2.1 is stronger than state-copy access but different from the classical ℓ^2 sample-and-query model. A block encoding is a coherent unitary access mechanism; it need not reveal entries, row norms, or efficient classical samples from squared amplitudes. Conversely, for low-rank matrices stored in sample-query data structures, quantum-inspired algorithms can dequantize important linear-algebra outputs [46, 47, 48, 49]. Section 10 states the corresponding access boundary.

3 Sharp compression of the optimal score readout

This section proves Result R1 at an SLD-regular operating point satisfying Eq. (12). Its basic variable is not the number of SLD eigenvectors but the probability measure of their scores under the state,

$$L = \sum_a \lambda_a \Pi_a, \qquad \nu_{\rho,L}(\Omega) = \mathrm{Tr}[\rho\, \mathbf{1}_\Omega(L)]. \tag{27}$$

The measure has unit mass and second moment

$$\int \lambda^2 \nu_{\rho,L}(\mathrm{d}\lambda) = F_Q. \tag{28}$$

For a spectral partition $\mathcal{I} = (I_b)_b$, define

$$B_b = \mathbf{1}_{I_b}(L), \quad q_b = \mathrm{Tr}(\rho B_b), \quad \bar{\ell}_b = \frac{\mathrm{Tr}(\dot{\rho} B_b)}{q_b} \tag{29}$$

for occupied bins. Empty bins also vanish exactly: $q_b = 0$ implies $B_b \preceq \Pi_0$, hence

$$\mathrm{Tr}(\dot{\rho} B_b) = \mathrm{Tr}(\Pi_0 \dot{\rho} \Pi_0 B_b) = 0 \tag{30}$$

Table 1: Objects and scope. Few-outcome readout is support robust; landscape geometry and the coherent compiler have additional assumptions.

Object	Definition	Role and assumptions
QFI	$F_Q = \mathrm{Tr}(\rho L^2)$	Optimal local information value at an SLD-regular operating point.
Score measure	$\nu_{\rho,L}(\Omega) = \mathrm{Tr}[\rho \mathbf{1}_\Omega(L)]$	Carries all spectral readout information; Result R1 needs no condition number.
Measurement score	$L_P = \sum_{q_j>0}(r_j/q_j)P_j$	Gives the exact residual certificate; benign critical-point geometry currently assumes $\rho > 0$.
Block encoding of L	Top-left block proportional to L	Supports coherent spectral processing under Assumption 2.1.
Implemented score instrument	V, (P_y), C, and $\xi = \|CV - V\widetilde{L}\|_\infty$	Actual finite-resolution POVM and uniform complexity-theoretic interface, including failure and leakage labels.

by Eq. (12). Since B_b commutes with L and $2\dot{\rho} = \rho L + L\rho$, every occupied bin satisfies

$$\bar{\ell}_b = \frac{\mathrm{Tr}(\rho L B_b)}{q_b} = \mathbb{E}_{\nu_{\rho,L}}[\lambda \mid I_b]. \tag{31}$$

Thus the optimal representative of a score cell is its conditional mean, while empty cells contribute neither probability nor tangent weight.

Theorem 3.1 (Score-projection identity and sharp diameter bound)**.** *The Fisher information $J_\mathcal{I} = \sum_b q_b \bar{\ell}_b^2$ of the coarse SLD PVM satisfies*

$$F_Q - J_\mathcal{I} = \sum_b q_b \,\mathrm{Var}_{\nu_{\rho,L}(\cdot|I_b)}(\lambda) \tag{32}$$

$$= \sum_b \mathrm{Tr}[\rho B_b (L - \bar{\ell}_b)^2]$$

$$\leq \frac{1}{4} \sum_b q_b \,\mathrm{diam}(I_b)^2. \tag{33}$$

The factor $1/4$ is sharp.

Proof. Equation (28) and the conditional-mean identity (31) give the law of total variance. Popoviciu's inequality bounds a variance supported on an interval of diameter Δ_b by $\Delta_b^2/4$, with equality for equal mass at the endpoints. ☐

Corollary 3.2 (Tight finite resolution)**.** *If every occupied score bin has diameter at most δ, then*

$$0 \leq F_Q - J_\delta \leq \frac{\delta^2}{4}. \tag{34}$$

If the occupied score spectrum has width W, K equal-width bins obey

$$F_Q - J_K \leq \frac{W^2}{4K^2}. \tag{35}$$

Both statements hold for faithful, pure, and rank-deficient states at SLD-regular operating points.

The next theorem avoids the full spectral width. Let

$$T_R := \int_{|\lambda|>R} \lambda^2 \nu_{\rho,L}(\mathrm{d}\lambda). \tag{36}$$

Theorem 3.3 (Tail-adaptive score compression)**.** *For every $R > 0$ and integer $K \geq 1$, a spectral PVM with at most $K+2$ outcomes satisfies*

$$F_Q - J_{K+2} \leq T_R + \frac{R^2}{K^2}. \tag{37}$$

If $T_R < \epsilon F_Q$, then $K \geq R/\sqrt{\epsilon F_Q - T_R}$ central cells plus two tail cells retain at least $(1-\epsilon)F_Q$.

Proof. Partition $[-R, R]$ into K intervals of width $2R/K$ and use one bin for each tail. Corollary 3.2 bounds the central loss by R^2/K^2. Each tail conditional variance is no larger than its unconditional second moment. ☐

The theorem is dimension free. It controls output alphabet and phase precision, not the circuit complexity of realizing the global projectors. Section 10 places the projection identity and the classical bounded-variance coefficient relative to prior work. We claim the support-aware SLD detector corollary, tail construction, and their integration with the compiler workflow, not priority for conditional variance or Popoviciu's constant.

3.1 Optimal quantization and the finite-support crossover

For a probability measure ν with finite second moment, define

$$D_K(\nu) = \inf_{|C|\leq K} \int \mathrm{dist}(\lambda, C)^2 \nu(\mathrm{d}\lambda). \tag{38}$$

Every scalar optimum obeys the Max–Lloyd centroid and nearest-neighbor conditions, but those stationary conditions are not sufficient for global optimality [61, 62, 63, 64]. In the present problem,

$$F_Q - J_K^\star = D_K(\nu_{\rho,L}). \tag{39}$$

At fixed finite dimension, the score measure has support size $m \leq d$, so

$$D_K(\nu_{\rho,L}) = 0 \qquad (K \geq m). \tag{40}$$

A continuous-density high-rate law can therefore describe only a joint dense-spectrum and large-K limit.

Lemma 3.4 (Wasserstein stability)**.** *For probability measures μ, ν with finite second moments,*

$$\left|\sqrt{D_K(\mu)} - \sqrt{D_K(\nu)}\right| \le W_2(\mu, \nu). \tag{41}$$

This constant-one root-distortion inequality is anteceded by the fixed-grid result of Liu and Pagès [65]; the short proof is included to fix notation.

Proof. For a codebook C, the distance-to-set function is 1-Lipschitz. Apply Minkowski's inequality to any coupling (X, Y) of μ and ν, then minimize over couplings and codebooks; exchange μ and ν for the reverse inequality. □

Corollary 3.5 (Dense-spectrum high-rate window)**.** *Let finite atomic score measures ν_n have support cardinalities $m_n := \#\operatorname{supp}\nu_n \to \infty$ and satisfy $W_2(\nu_n, \nu) \to 0$, where $\nu = f(\lambda)\mathrm{d}\lambda$ has a compactly supported density continuous and positive on the interior of its support. If*

$$K_n \to \infty, \qquad K_n < m_n, \qquad K_n W_2(\nu_n, \nu) \to 0, \tag{42}$$

then

$$K_n^2\big(F_Q^{(n)} - J_{K_n}^{\star,(n)}\big) \longrightarrow \frac{1}{12}\left(\int f(\lambda)^{1/3}\mathrm{d}\lambda\right)^3. \tag{43}$$

For each finite n, the distortion instead becomes exactly zero at $K \ge m_n$.

Proof. The rigorous one-dimensional squared-error quantization theorem of Graf and Luschgy, Theorem 6.2, gives the limit for $D_K(\nu)$ and the constant $1/12$; Panter–Dite and Zador provide the historical high-resolution antecedents [66, 67, 68, 63, 64]. Multiplying Eq. (41) by K_n and using $K_n W_2(\nu_n, \nu) \to 0$ transfers the square-root distortion to ν_n. Squaring and applying Eq. (39) proves the result. □

For a finite sorted spectrum, the exact best contiguous partition is classical one-dimensional dynamic programming. If $w_a = \mathrm{Tr}(\rho\Pi_a)$, the interval cost is

$$C(i,j) = \sum_{a=i}^{j-1} w_a\lambda_a^2 - \frac{\left(\sum_{a=i}^{j-1} w_a\lambda_a\right)^2}{\sum_{a=i}^{j-1} w_a}, \tag{44}$$

and the Bellman recursion

$$D(k,j) = \min_{i<j}\{D(k-1,i) + C(i,j)\} \tag{45}$$

finds the optimum in $O(Kd^2)$ time [69, 70]. We use this established algorithm as an exact numerical oracle. Figure 1(c,d) tests the tail and sharp-resolution theorems; Supplemental Fig. S4 tests the intermediate high-rate window and terminal atomic crossover.

4 Exact Fisher certificate and benign projective search

Result R2 has two logically distinct ingredients. The exact residual identity is elementary and is proved here. The nonconvex critical-point geometry is imported from the companion Landscape paper [6]; none of its general theorems or proofs is reproduced.

4.1 Three-line residual identity

Proposition 4.1 (Exact Fisher residual for orthogonal measurements)**.** *At every SLD-regular operating point, let $\mathcal{B} = (B_b)_b$ be any orthogonal resolution of the identity. For occupied cells define*

$$q_b = \mathrm{Tr}(\rho B_b), \qquad r_b = \mathrm{Tr}(\dot\rho B_b), \qquad \bar\ell_b = r_b/q_b, \tag{46}$$

and set

$$J(\mathcal{B}) = \sum_{b:q_b>0}\frac{r_b^2}{q_b}, \qquad L_{\mathcal{B}} = \sum_{b:q_b>0}\bar\ell_b B_b. \tag{47}$$

Then

$$F_Q - J(\mathcal{B}) = \mathrm{Tr}[\rho(L_{\mathcal{B}} - L)^2]. \tag{48}$$

In particular, a rank-one PVM gives $J(\mathcal{B}) = J(P)$ and $L_{\mathcal{B}} = L_P$.

Proof. Orthogonality gives $\mathrm{Tr}(\rho L_{\mathcal{B}}^2) = J(\mathcal{B})$. Using $\rho L + L\rho = 2\dot\rho$,

$$\begin{aligned}\mathrm{Tr}[\rho(L_{\mathcal{B}} - L)^2] &= J(\mathcal{B}) - \mathrm{Tr}[(\rho L + L\rho)L_{\mathcal{B}}] + F_Q \\ &= J(\mathcal{B}) - 2\,\mathrm{Tr}(\dot\rho L_{\mathcal{B}}) + F_Q = F_Q - J(\mathcal{B}),\end{aligned} \tag{49}$$

because $\mathrm{Tr}(\dot\rho L_{\mathcal{B}}) = \sum_b r_b\bar\ell_b = J(\mathcal{B})$. Empty cells have $q_b = r_b = 0$ by Eqs. (12) and (30), so the restricted sums are exact. □

For rank-one PVMs, Eq. (48) is the Pythagorean completion behind the Braunstein–Caves inequality and its equality conditions [3, 4]. We make no priority claim for that inequality or projection principle. Its role here is operational: the measured Fisher deficit is exactly a state-weighted score residual, which becomes both a stopping rule and the bridge to the cited nonconvex geometry.

4.2 Dictionary to the companion Landscape theorem

For nonzero ε such that

$$\rho_\varepsilon = \rho + \varepsilon\dot\rho > 0, \tag{50}$$

consider the quadratic divergence generated by $h(t) = (t-1)^2$. Every rank-one PVM obeys the exact reduction

$$D_{\chi^2}(p_{\rho_\varepsilon}^P \| p_\rho^P) = \sum_j q_j\left(\frac{q_j + \varepsilon r_j}{q_j} - 1\right)^2 = \varepsilon^2 J(P). \tag{51}$$

The projective score variable of Ref. [6] becomes

$$\Gamma_P = I + \varepsilon L_P, \qquad \Gamma_\star = I + \varepsilon L, \tag{52}$$

and equal likelihood-ratio blocks are exactly equal Fisher-score blocks.

Invoking the companion score-block and pair-rotation theorems gives the following metrological specialization.

Corollary 4.2 (Benign Fisher-measurement landscape). *Let $\rho > 0$ and $\dot\rho = \dot\rho^\dagger$ with $\operatorname{Tr}\dot\rho = 0$. At a critical rank-one PVM, write*

$$L_P = \sum_{\alpha=1}^{m} \ell_\alpha B_\alpha \tag{53}$$

with distinct scores. The PVM is globally optimal over all POVMs if and only if

$$B_\alpha(\dot\rho - \ell_\alpha\rho)B_\alpha = 0 \qquad \text{for every } \alpha. \tag{54}$$

If this condition fails, some equal-score block contains basis vectors $j \neq k$ and a phase-adjusted two-vector rotation satisfying

$$\frac{\mathrm{d}^2}{\mathrm{d}t^2} J(P(t))\bigg|_{t=0} = 8\,|\langle j|(\dot\rho - \ell_\alpha\rho)|k\rangle|^2 \left(\frac{1}{q_j} + \frac{1}{q_k}\right) > 0. \tag{55}$$

Consequently every projective local maximum and every second-order stationary PVM is globally optimal over all POVMs, and every nonglobal critical PVM has an explicit strict-ascent pair rotation.

The block residual follows directly from the dictionary,

$$B_\alpha[\rho_\varepsilon - (1+\varepsilon\ell_\alpha)\rho]B_\alpha = \varepsilon B_\alpha(\dot\rho - \ell_\alpha\rho)B_\alpha. \tag{56}$$

All global-optimality and escape conclusions in Corollary 4.2 belong to Ref. [6]; the present paper contributes only the Fisher dictionary and its operational use. In particular, if a critical PVM has distinct scores, every block is rank one and the imported condition is automatically satisfied.

Corollary 4.2 is an exact statement about search on the physical flag manifold. It excludes bad stationary maxima but does not provide a dimension-independent convergence rate, a gradient lower bound away from stationarity, or robustness to ansatz restriction and sampling noise. The next section records the conditioned linear score-space baseline used to interpret the coherent compiler.

5 Conditioning of the SLD score equation

The SLD is the unique maximizer, for faithful ρ, of the quadratic potential

$$\Phi(X) = 2\operatorname{Tr}(\dot\rho X) - \operatorname{Tr}(\rho X^2), \tag{57}$$

whose Hilbert–Schmidt gradient is

$$\nabla\Phi(X) = 2\dot\rho - \rho X - X\rho. \tag{58}$$

Completing the square gives

$$\Phi(L) - \Phi(X) = \operatorname{Tr}[\rho(X-L)^2]. \tag{59}$$

This section records the classical conditioning baseline. The iteration below is standard Richardson iteration, not a new algorithmic result.

Assume

$$\mu I \preceq \rho \preceq \Lambda I, \qquad \kappa = \Lambda/\mu. \tag{60}$$

The Sylvester superoperator $\mathcal{S}_\rho(X) = \rho X + X\rho$ is positive self-adjoint with spectrum in $[2\mu, 2\Lambda]$.

Proposition 5.1 (Exact score conditioning). *For every Hermitian X,*

$$\mu\|X-L\|_2^2 \le \Phi(L) - \Phi(X) \le \Lambda\|X-L\|_2^2, \tag{61}$$

$$4\mu[\Phi(L)-\Phi(X)] \le \|\nabla\Phi(X)\|_2^2 \le 4\Lambda[\Phi(L)-\Phi(X)]. \tag{62}$$

Corollary 5.2 (Richardson/Jacobi baseline). *The update*

$$X_{m+1} = X_m + \frac{2\dot\rho - \rho X_m - X_m\rho}{\mu+\Lambda} \tag{63}$$

obeys

$$\begin{aligned} &\|X_m - L\|_2 \le r^m\|X_0 - L\|_2, \\ &\Phi(L) - \Phi(X_m) \le r^{2m}[\Phi(L) - \Phi(X_0)], \qquad r = \frac{\kappa-1}{\kappa+1}. \end{aligned} \tag{64}$$

Proof. In an eigenbasis of ρ, each error mode is multiplied by

$$1 - \frac{\lambda_i + \lambda_j}{\mu+\Lambda}. \tag{65}$$

Since $\lambda_i + \lambda_j \in [2\mu, 2\Lambda]$, the maximum magnitude is $(\kappa-1)/(\kappa+1)$. Equations (61) and (62) follow from the same diagonalization; Appendix A gives the full mode calculation. □

The continuous flow

$$\dot X_t = 2\dot\rho - \rho X_t - X_t\rho \tag{66}$$

satisfies $\mathrm{d}\Phi(X_t)/\mathrm{d}t = \|\nabla\Phi(X_t)\|_2^2$ and, for $X_0 = 0$,

$$X_t = 2\int_0^t e^{-s\rho}\dot\rho e^{-s\rho}\mathrm{d}s \longrightarrow L. \tag{67}$$

Storing this dense iterate costs $O(d^2)$ classical memory. Its purpose here is to expose the condition number shared by classical and quantum Sylvester methods.

The metrological connection is exact. For a physical measurement score,

$$\Phi(L) - \Phi(L_P) = F_Q - J(P) \tag{68}$$

by Proposition 4.1. Thus an operator-space error estimate becomes a Fisher-information guarantee without an extra Lipschitz relaxation. The coherent compiler uses a different solver but targets the same fixed point.

6 Coherent SLD interface and error budget

This section separates the matrix layer from the implemented measurement layer. Established quantum linear-matrix methods provide an approximate block encoding of the SLD under the promised access model [45]. Spectral-processing primitives can then be used to build a label circuit [54, 55, 56, 57]. Sheng's contemporaneous record-compression theorem already identifies a state-weighted Stinespring score-intertwining defect whose square is the exact QFI loss [71]. We claim no priority for that foundational identity. The contribution here is to impose a uniform operator-norm version as a delivered compiler interface, separate matrix and implementation errors, allow declared-score mismatch on exhaustive failure and leakage labels, transport the same interface into reconstructed-signal error, and compose it with the SLD and hardness constructions. The quoted primitive cost remains conditional on certifying that uniform interface.

6.1 From a Sylvester solution to a declared interface

Under the common scaling $S = c\rho$ and $D = c\dot{\rho}$,

$$SL + LS = 2D. \tag{69}$$

Normalize it as

$$\frac{S}{2\Lambda}L + L\frac{S}{2\Lambda} = \frac{D}{\Lambda}. \tag{70}$$

The coefficient spectrum lies in $[1/(2\kappa), 1/2]$. Under Assumption 2.1, SLBB constructs a block encoding of an approximation $\widetilde{L}/x$ with

$$x = \widetilde{O}(\alpha\kappa) \tag{71}$$

and $\widetilde{O}(\sqrt{\kappa})$ coefficient-oracle queries in the positive-square-root access model [45]. Qubitization and phase-estimation methods resolve scores using $O(x/\delta)$ calls at a declared numerical resolution, subject to the accuracy and failure guarantees of the chosen primitive [54, 55, 56, 57, 72]. Combining these quoted layers suggests the conditional scaling

$$Q_{\text{matrix+spectral}} = \widetilde{O}\left(\frac{\alpha\kappa^{3/2}}{\delta}\right). \tag{72}$$

Equation (72) is a primitive-layer query expression. It is an end-to-end compiler bound only when the implementation supplies the uniform contract below at the requested cost. Promised block encodings and all normalizations must also have polynomial-resource constructions for the dependence to be polynomial in the qubit count.

Algorithm 6.1 (Operational SLD compiler contract)**.** *Input: Block encodings satisfying Assumption 2.1; a matrix tolerance η; exhaustive label projectors $(P_y)_y$; bounded declared scores $(c_y)_y$; and a target score-intertwining defect ξ.*

1. *Normalize the SLD equation as in Eq. (70) and construct a Hermitian approximation $\widetilde{L}$ satisfying*

$$\|\widetilde{L} - L\|_\infty \le \eta. \tag{73}$$

2. *Apply a parameter-independent coherent spectral routine to obtain the actual initialized isometry V. Include ordinary, boundary, leakage, and failure labels in the exhaustive family $(P_y)_y$.*

3. *Define $C = \sum_y c_y P_y$ and certify the uniform output contract*

$$\|CV - V\widetilde{L}\|_\infty \le \xi. \tag{74}$$

4. *Output the implemented POVM $M_y = V^\dagger P_y V$ together with C, η, ξ, and the evidence supporting Eqs. (73)–(74).*

The contract in Eq. (74) is stable under bin-boundary relabeling when every assigned score remains close to the represented eigenvalue. A failure-probability statement alone does not imply it: the failure branch needs a declared score, and the error must be uniform over inputs for the later hardness reduction.

6.2 Exact approximate-operator PVM

Suppose Eq. (73) holds and the exact spectrum of $\widetilde{L}$ is grouped into bins of width at most δ.

Theorem 6.2 (Exact approximate-operator PVM loss)**.** *If $\mu I \preceq \rho \preceq \Lambda I$ and $\kappa = \Lambda/\mu$, the exact coarse spectral PVM of $\widetilde{L}$ satisfies*

$$F_Q - J_{\delta,\widetilde{L}} \le \min\left\{(\kappa+1)^2\eta^2 + \frac{(\delta+2\kappa\eta)^2}{4},\ \left[\delta + (\kappa+1)\eta\right]^2\right\}. \tag{75}$$

At $\eta = 0$ this is the sharp $\delta^2/4$ law; at $\delta = 0$ the second branch gives $(\kappa+1)^2\eta^2$.

Proof. For a $\widetilde{L}$ eigenvector $|j\rangle$ with eigenvalue $\widetilde{\lambda}_j$, the SLD equation gives

$$\ell_j - \widetilde{\lambda}_j = \frac{\langle j|[\rho(L-\widetilde{L}) + (L-\widetilde{L})\rho]|j\rangle}{2q_j}, \tag{76}$$

so $|\ell_j - \widetilde{\lambda}_j| \le \kappa\eta$. Therefore the refined score operator obeys $\|L_P - L\|_\infty \le (\kappa+1)\eta$, and Proposition 4.1 gives $F_Q - J(P) \le (\kappa+1)^2\eta^2$. Within one approximate bin, the exact scores have range at most $\delta + 2\kappa\eta$; Theorem 3.1 bounds the additional merging loss, proving the first branch.

For the second branch, the coarse score operator $L_{\mathcal{B}} = \sum_b \bar{\ell}_b B_b$ satisfies $\|L_{\mathcal{B}} - L\|_\infty \le \delta + (\kappa+1)\eta$. Applying Proposition 4.1 directly gives the second branch. ☐

Theorem 6.2 concerns exact spectral projectors of $\widetilde{L}$. The implemented circuit is governed separately by the following result.

Equation (78) below is the declared-score form of the Stinespring QFI-loss identity in Ref. [71]; our norm bound is its direct uniform corollary after separating η from ξ.

Theorem 6.3 (Implemented score-interface loss)**.** *Let V, $(P_y)_y$, C, and ξ satisfy the operational contract of Algorithm 6.1. For the actual POVM $M_y = V^\dagger P_y V$,*

$$F_Q - J(M) \le (\eta + \xi)^2. \tag{77}$$

Proof. For every occupied label define $q_y = \operatorname{Tr}(\rho M_y)$, $r_y = \operatorname{Tr}(\dot{\rho} M_y)$, and $\ell_y = r_y/q_y$. Put $G = CV - VL$. Expanding $G^\dagger G$ and using $2\dot{\rho} = \rho L + L\rho$ gives the exact identity

$$\operatorname{Tr}(\rho G^\dagger G) = F_Q - J(M) + \sum_{y:q_y>0} q_y (c_y - \ell_y)^2. \tag{78}$$

The sum is nonnegative. Moreover,

$$\|G\|_\infty \le \|CV - V\widetilde{L}\|_\infty + \|V(\widetilde{L} - L)\|_\infty \le \xi + \eta. \tag{79}$$

Since V is an isometry and $\operatorname{Tr}\rho = 1$, Eq. (77) follows. □

Corollary 6.4 (Reconstructed signal operator)**.** *Suppose a controlled signal gadget has declared scale $s > 0$ and actual top-left label block K satisfying*

$$\|K - sC\|_\infty \le \chi. \tag{80}$$

Conjugating by the same actual implemented circuit and its inverse gives the initialized-ancilla signal block $V^\dagger K V$. The reconstructed operator

$$L_c = \frac{V^\dagger K V}{s} \tag{81}$$

satisfies

$$\|L_c - L\|_\infty \le \eta + \xi + \frac{\chi}{s}. \tag{82}$$

Theorem 6.3 and Corollary 6.4 provide the operational bridge needed by the measurement and hardness statements. They certify consequences of a delivered interface. Establishing Eq. (74) from a particular finite-precision primitive, including its worst-case failure and score-range bounds, is a separate implementation obligation.

7 BQP-hard compilation with full SLD support

SLBB already showed that unrestricted quantum Sylvester equations can encode BQP-complete computation [45]. Result R3 asks a narrower question: do trace normalization, positivity, faithfulness, polynomial conditioning, finite score resolution, and nonnegligible metrological weight make coherent SLD synthesis easier? The following embedding shows that they do not.

7.1 Coherent synthesis task

The input is a faithful differentiable state family satisfying Assumption 2.1. The output is the operational score interface of Eqs. (21)–(24): a parameter-independent initialized isometry V, exhaustive label projectors, a bounded score operator C, and a uniform defect ξ. A declared controlled signal gadget then yields the reconstructed operator of Corollary 6.4. The hardness task requires

$$\eta + \xi + \chi/s \le \frac{\epsilon_{\mathrm{QLS}}}{4\kappa} \tag{83}$$

for an inverse-polynomial requested ϵ_{QLS}. This coherent action on chosen inputs is a stronger output than drawing a classical outcome from the sensor state. Exact inversion of the actual circuit reconstructs its own signal block; Corollary 6.4 supplies the additional proximity to L.

Positive quantum linear systems remain BQP-hard under block-encoding access [73, 74]. Let $A > 0$ have spectrum in $[1/\kappa_A, 1]$, abbreviate κ_A by κ within the embedding, let $|b\rangle$ be normalized, and let U_b be an efficient state-preparation unitary with $U_b|0\rangle = |b\rangle$. Set

$$a = \frac{1}{2\kappa}, \qquad \gamma = \frac{a}{2}. \tag{84}$$

On $\mathcal{H}_1 \oplus \mathcal{H}_2$, define

$$S = \begin{pmatrix} A - aI & 0 \\ 0 & aI \end{pmatrix}, \tag{85}$$

$$T = \gamma \begin{pmatrix} 0 & U_b \\ U_b^\dagger & 0 \end{pmatrix}, \tag{86}$$

$$\rho_\theta = \frac{S + \theta T}{Z}, \qquad Z = \operatorname{Tr} S = \operatorname{Tr} A. \tag{87}$$

Lemma 7.1 (Faithfulness and conditioning)**.** *For every $|\theta| \le 1$, ρ_θ is trace one and faithful. Moreover,*

$$aI \preceq S \preceq (1-a)I, \qquad \kappa(\rho_0) \le 2\kappa - 1. \tag{88}$$

Proof. The first block $A - aI$ has spectrum in $[a, 1-a]$ and the second equals aI, so $S \succeq aI$. The off-diagonal unitary block has norm one, hence $\|T\| = \gamma = a/2$. Weyl's inequality gives, for every $|\theta| \le 1$,

$$S + \theta T \succeq (a - |\theta|\gamma)I = a\left(1 - \frac{|\theta|}{2}\right) I \succeq \frac{a}{2} I > 0. \tag{89}$$

Also $\operatorname{Tr} T = 0$, proving trace normalization and faithfulness. The lower bound $a/2$ is the positivity margin tested numerically in Eq. (111). □

At $\theta = 0$, normalization cancels from the SLD equation. Its unique solution is

$$L = \begin{pmatrix} 0 & aA^{-1}U_b \\ aU_b^\dagger A^{-1} & 0 \end{pmatrix}, \tag{90}$$

because the upper-right block X satisfies

$$(A - aI)X + XaI = AX = aU_b. \tag{91}$$

The singular values of X are $a/\lambda_i(A)$, so

$$\operatorname{spec}(L) = \left\{ \pm \frac{a}{\lambda_i(A)} \right\}_{i=1}^{N}, \qquad a \le |\lambda(L)| \le \frac{1}{2}. \quad (92)$$

The SLD has no zero sector: its nonzero spectral weight under ρ_0 is exactly one. Its zero-score margin is therefore

$$g_0(L) = \min_{\lambda \in \operatorname{spec}(L)} |\lambda| = \frac{a}{\lambda_{\max}(A)} \ge a = \frac{1}{2\kappa}. \quad (93)$$

No lower bound on the spacing between two distinct nonzero scores is asserted or needed.

The QFI is inverse polynomial:

$$F_Q = \frac{a^2 \operatorname{Tr}(A^{-1})}{\operatorname{Tr} A}, \qquad \frac{1}{4\kappa^2} \le F_Q \le \frac{1}{4}. \quad (94)$$

The formula follows by multiplying S with L^2; the bounds use $1/\kappa \le A \le I$.

The scaled lower bounds have a simple tightness characterization. Cauchy–Schwarz gives

$$4\kappa^2 F_Q = \frac{\operatorname{Tr}(A^{-1})}{\operatorname{Tr} A} \ge \frac{N^2}{(\operatorname{Tr} A)^2} \ge 1, \quad (95)$$

with equality only at $A = I$; similarly, $\kappa^2 p_{\text{app}} = \|A^{-1}b\|^2 \ge 1$. Near-identity matrices are therefore the appropriate numerical probes of both lower bounds.

Theorem 7.2 (Full-support faithful-model hardness)**.** *Coherent SLD score-interface synthesis satisfying Eq. (83) is BQP-hard even for one-parameter density-operator models that*

(i) are trace one and faithful for every $|\theta| \le 1$;

(ii) satisfy $\kappa(\rho_0) \le 2\kappa - 1$;

(iii) have full SLD support with zero-score margin $g_0(L) \ge 1/(2\kappa)$; and

(iv) have $F_Q \ge 1/(4\kappa^2)$.

The algebraic reduction and requested accuracy are polynomially conditioned. Quantum-polynomial-time membership through Algorithm 6.1 is conditional on a spectral-processing primitive that certifies the uniform interface at its quoted cost.

Proof. Let V be the actual initialized isometry and let C contain the declared scores of every label. Scores are clipped to $[-1/2, 1/2]$, with the clipping contribution charged in ξ, so a label-controlled signal gadget can have top-left block K satisfying $\|K - 2C\|_\infty \le \chi$. Conjugation by the same implemented circuit and its inverse gives the exact initialized-ancilla signal block $V^\dagger K V$. Define

$$L_c = \frac{1}{2} V^\dagger K V, \qquad \tau = \|L_c - L\|_\infty \le \eta + \xi + \frac{\chi}{2}. \quad (96)$$

Postselecting the signal ancilla applies $2L_c$ to the chosen input. The exact operator obeys

$$L|2,0\rangle = a|1\rangle\, A^{-1} U_b |0\rangle = a|1\rangle\, A^{-1}|b\rangle. \quad (97)$$

The exact signal success probability is

$$p_{\text{app}} = 4a^2 \|A^{-1}b\|^2 \ge \frac{1}{\kappa^2}, \quad (98)$$

and the implemented success probability is bounded by

$$p_{\text{app}}^{\text{impl}} \ge (1/\kappa - 2\tau)^2. \quad (99)$$

For $\tau < 1/(2\kappa)$ the output is nonzero, and the normalized vector error is at most $4\kappa\tau$. Equation (83) therefore gives error at most ϵ_{QLS} and, for $\epsilon_{\text{QLS}} \le 1$, leaves success at least $1/(4\kappa^2)$. Amplitude amplification remains polynomial. Positive QLS is BQP-hard, and the block encodings of S, T plus square-root access are constructed with polynomial overhead from those of A and U_b; Appendix D gives the full access reduction. This proves BQP-hardness for the declared coherent score-interface task. The primitive-to-interface implementation cost remains the conditional boundary identified in Sec. 6. ☐

If the positive instance is obtained from a Hermitian QLS matrix H of condition number κ_H by the normal-equations reduction $A = H^2$, then $\kappa_A \le \kappa_H^2$. In the original parameter, the embedding therefore guarantees

$$\kappa(\rho_0) \le 2\kappa_H^2 - 1, \qquad g_0(L) \ge \frac{1}{2\kappa_H^2},$$
$$F_Q \ge \frac{1}{4\kappa_H^4}, \qquad p_{\text{app}} \ge \frac{1}{\kappa_H^4}. \quad (100)$$

The theorem's novelty is the survival of hardness under the listed metrological restrictions, not the general hardness of the Sylvester primitive. The full-support construction also removes the earlier objection that the QLS-bearing sector was exponentially rare.

7.2 Scope of the hardness statement

The hardness concerns the compiled coherent map on chosen inputs. It does not prove that ordinary SLD-outcome samples from ρ_0 are BQP-hard. If $A|v_i\rangle = \lambda_i|v_i\rangle$, the SLD eigenvectors are

$$|\pm, i\rangle = \frac{|1, v_i\rangle \pm |2, U_b^\dagger v_i\rangle}{\sqrt{2}}, \quad (101)$$

and their sensor-state probabilities are

$$\operatorname{Tr}(\rho_0 |\pm, i\rangle\langle \pm, i|) = \frac{\lambda_i}{2 \operatorname{Tr} A}. \quad (102)$$

These statistics have full support but do not depend on the right-hand side $|b\rangle$. This is a positive separation of output notions: the entire marginal score histogram is classically insensitive to the encoded QLS right-hand side, while the SLD eigenvectors retain it coherently. The quantum advantage in the reduction is therefore not finer classical score resolution; it is access to the coherent spectral instrument and its action on selected inputs. Result R3 is stated at exactly that level.

8 Numerical validation

This section reports deterministic audits of Results R1–R4. The calculations test identities, constants, promise constructions, and finite-dimensional resource ledgers; they are not substitutes for the asymptotic reductions. Dense random-state linear algebra supplies reference values through $d = 64$, an exactly solvable dense-spectrum sequence reaches $d = 256$, and the parity-coherence family is evaluated analytically through $n = 128$. All panels and tables are regenerated from archived machine-readable data with master seed 20260818. Appendix E specifies the ensembles and thresholds.

8.1 Projective geometry and the exact residual

The three-level instance

$$\rho = I/3, \qquad \dot{\rho} = \begin{pmatrix} 0.1 & 0.2 & 0 \\ 0.2 & 0.1 & 0 \\ 0 & 0 & -0.2 \end{pmatrix} \tag{103}$$

has computational-basis scores $(0.3, 0.3, -0.6)$. The equal-score block has off-diagonal residual 0.2, $J = 0.18$, and $F_Q = 0.42$. The pair-rotation formula imported in Result R2 predicts

$$8(0.2)^2(3+3) = 1.92, \tag{104}$$

while a central finite difference gives 1.9199997; a transverse inter-block rotation has curvature -1.0800005. Figure 1(a) therefore resolves a genuine nonglobal saddle.

For 600 PVMs in $d = 16$ with $\kappa(\rho) = 8$, we compared the two sides of

$$F_Q - J(P) = \mathrm{Tr}[\rho(L_P - L)^2]. \tag{105}$$

The ensemble combines geodesic perturbations of an SLD eigenbasis with Haar-random PVMs and spans more than eight decades of suboptimality. Figure 1(b) shows the identity line above the points; the maximum absolute discrepancy is 8.59×10^{-18}.

8.2 Score compression

We evaluated the exact contiguous Lloyd–Max quantizer of Eq. (45) on 20 independent models for each $d \in \{8, 16, 32, 64\}$. Figure 1(c) compares the exact bin count retaining 99% of F_Q with the constructive count obtained from Theorem 3.3 using each instance's measured T_R. The exact medians are $7, 10, 12, 14$ bins; the theorem guarantees $25.5, 28, 30, 31.5$. Over this tested range only,

$$\begin{aligned} K_{99}^{\star} &= 7.3 + 2.3\log_2(d/8), \qquad & R^2 &= 0.989, \\ K_{99}^{\mathrm{tail}} &= 25.8 + 2.0\log_2(d/8), \qquad & R^2 &= 0.988. \end{aligned} \tag{106}$$

This is a finite-range trend, not an asymptotic sublinear-in-d claim.

The tail theorem was tested constructively on the four-spin model at $\beta = 0.30$. For $R \in \{0.5, 1, 1.5, 2\}$ and $K \in \{4, 8\}$, we used exactly the central-uniform-plus-two-tail partition from its proof. Across all eight tests,

$$\max \frac{F_Q - J_{K+2}}{T_R + R^2/K^2} = 0.323037 < 1. \tag{107}$$

Supplemental Fig. S3(a) shows the losses against their instance-specific budgets.

The dense-spectrum gate uses the commuting models

$$\begin{aligned} \lambda_j^{(m)} &= -1 + \frac{2j-1}{m}, \qquad j = 1, \ldots, m, \\ \rho_m &= I/m, \qquad L_m = \mathrm{diag}(\lambda_j^{(m)}), \\ \dot{\rho}_m &= L_m/m. \end{aligned} \tag{108}$$

For $K \mid m$,

$$D_K(\nu_m) = \frac{1}{3K^2} - \frac{1}{3m^2}. \tag{109}$$

Thus $K^2 D_K$ approaches $1/3$ in the intermediate window and $D_m = 0$ exactly. For $m = 64, 128, 256$, the maximum archived intermediate relative deviation is 0.015625, the exact-formula error is 0, and the terminal loss is 0; Supplemental Fig. S4(a) displays both regimes.

For 40 random $d = 32$, $\kappa = 8$ models, the SLD spectrum was binned at 13 requested resolutions. Each record uses the actual occupied-bin diameter and the sharp budget $\delta^2/4$. The largest observed ratio is

$$\max \frac{F_Q - J_\delta}{\delta^2/4} = 0.366541 < 1. \tag{110}$$

Figure 1(d) plots loss against theorem budget; points above the diagonal are forbidden by Result R1.

8.3 Conditioning, full-support hardness, and scalable sensing

For the standard Richardson diagnostic, we generated 20 random $d = 32$ models at each $\kappa \in \{2, 4, 8, 16\}$ and used the exact step $1/(\mu + \Lambda)$. At $\kappa = 16$, the median normalized potential gap after 90 iterations is 7.815×10^{-13}; Supplemental Fig. S1(c) compares the trajectories with the exact contraction envelope.

The full-support QLS embedding of Result R3 was tested on 123 positive instances with dimensions $4, 8, 16$. The suite contains interior spectra under the promises $\kappa = 2, 4, 8, 16, 32$ and three non-saturating near-identity instances at promised $\kappa = 1.05$. Across all instances,

$$\begin{aligned} \max \frac{\|SL + LS - 2T\|_2}{\|2T\|_2} &= 4.494 \times 10^{-15}, \\ \max \frac{\|L_{\text{num}} - L_{\text{exact}}\|_2}{\|L_{\text{exact}}\|_2} &= 4.203 \times 10^{-15}, \\ \min F_{\text{QLS}} &> 1 - 10^{-15}, \\ \min \kappa^2 p_{\text{app}} &= 1.047458, \\ \min 4\kappa^2 F_Q &= 1.060359, \\ \min[g_0(L)/a] &= 1.005487, \\ \min[\lambda_{\min}(S \pm T)/a] &= 0.500000. \end{aligned} \tag{111}$$

Every tested SLD has full nonzero spectral support. The near-identity subset brings $4\kappa^2 F_Q$ to 1.060359, close to its AM–HM lower bound. Its zero-score-margin ratio is 1.010101, whereas the closest score-margin ratio over the full suite, 1.005487, occurs in an interior-spectrum instance. Replacing $|b\rangle$ by an independent right-hand side at fixed A changes neither score locations nor sensor-state score probabilities beyond 3.220×10^{-15}. These are checks of the closed-form embedding and its promises; BQP-hardness follows from the reduction, not from sampling.

The promise-compatible parity family in Result R4 was evaluated through $n = 128$. It has exactly $\kappa = 3.0$, $F_Q = n/4$, and $n+1$ scores at every tested size; at $n = 128$, $F_Q = 32.0$ and the exact score register has 8 bits. Figure 3(d) displays the extensive-QFI and logarithmic-memory trends.

TABLE II. Selected archived numerical gates. The Supplemental Material reports 12 validation families comprising 34 executable checks; `reproduce.py` regenerates the data before `validate.py` applies the declared thresholds.

Gate	Threshold	Observed
Exact gap identity	$< 10^{-14}$	8.59×10^{-18}
Escape curvature	$< 10^{-6}$ error	2.85×10^{-7}
Richardson, $\kappa = 16$	$< 10^{-10}$	7.815×10^{-13}
Sharp resolution theorem	ratio ≤ 1	0.366541
Tail-adaptive theorem	ratio ≤ 1	0.323037
Dense-spectrum window	rel. error < 0.02; $D_m = 0$	0.015625; exact zero
Random $d = 64$, 99% compression	diagnostic	optimum / guarantee: 14/31.5
Full-support Sylvester residual	$< 10^{-12}$	4.494×10^{-15}
QLS output fidelity	$> 1 - 10^{-12}$	$> 1 - 10^{-15}$
Application success	$\kappa^2 p_{\text{app}} \geq 1$	1.047458
Inverse-polynomial QFI	$4\kappa^2 F_Q \geq 1$	1.060359
RHS-independent score histogram	error $< 10^{-12}$	3.220×10^{-15}
Product-PVM fraction	diagnostic	0.4855
Seven/eight score bins	$> 0.98/0.99$	0.9834/0.9926
Parity sensor	$\kappa = 3$, $F_Q = n/4$	exact through $n = 128$
Gibbs condition identity	rel. error $< 10^{-12}$	1.36×10^{-16}
Shrinking Gibbs window	$\kappa_{c=1} < 20$; $0.75 < nF_Q < 1.30$	17.56; 0.81–1.20

Together with Sec. 9, these gates support the archived finite-dimensional evidence in Result R4. They validate identities, constants, approximation budgets, and promise constructions after regeneration. They do not emulate a large coherent circuit or convert the four-spin benchmark into an asymptotic speedup instance.

9 Promise-compatible sensors and a frustrated thermal benchmark

Result R4 has two complementary physical messages. First, polynomial conditioning and nondecaying sensitivity coexist in an explicit scalable parity-coherence sensor. Second, Gibbs access has an exact conditioning obstruction that must be included in any resource claim. The Gibbs sensitivity study is finite size, and the four-spin model provides a nontrivial entangled-readout benchmark with an auditable data ledger.

9.1 A constant-conditioned extensive-QFI family

The state family below is unitarily equivalent to the partially polarized one-clean-qubit metrology construction of Cable, Gu, and Modi, which already establishes the underlying parity coherence and extensive $\epsilon^2 n$-type sensitivity [75]. We claim no priority for that probe family or scaling. The purpose here is the compiler-resource specialization: an explicit SLD, its commuting-generator decomposition, exact $n+1$ score alphabet, constant conditioning, and balanced-access representation.

Let

$$P_n = X^{\otimes n}, \qquad H_n = \frac{1}{2}\sum_{j=1}^{n} Z_j, \tag{112}$$

and, for fixed $0 < \epsilon < 1$, define the parity-coherence sensor

$$\rho_{n,\theta} = e^{-i\theta H_n} \frac{I + \epsilon P_n}{2^n} e^{i\theta H_n}. \tag{113}$$

It is a full-rank stabilizer-diagonal state subjected to a local collective phase rotation.

Proposition 9.1 (Conditioned extensive-QFI sensor)**.** *At $\theta = 0$, the family in Eq. (113) satisfies*

$$\kappa(\rho_{n,0}) = \frac{1+\epsilon}{1-\epsilon}, \tag{114}$$

$$L_n = -2i\epsilon H_n P_n = \epsilon \sum_{j=1}^{n} Y_j \prod_{k \neq j} X_k, \tag{115}$$

$$F_Q^{(n)} = \epsilon^2 n. \tag{116}$$

The n Pauli terms in L_n commute and are independent. Hence the exact SLD score has only $n+1$ distinct values $\epsilon(n-2k)$ and needs $\lceil \log_2(n+1) \rceil$ classical bits, although its eigenspaces resolve 2^n joint stabilizer patterns.

Proof. The eigenvalues of $I + \epsilon P_n$ are $1 \pm \epsilon$, proving Eq. (114). Since $P_n H_n P_n = -H_n$, the operator in Eq. (115) anticommutes with P_n and obeys

$$(I + \epsilon P_n)L_n + L_n(I + \epsilon P_n) = 2L_n = -2i\epsilon[H_n, P_n], \tag{117}$$

which is the scaled SLD equation. The Pauli strings $Q_j = Y_j \prod_{k \neq j} X_k$ commute pairwise and satisfy $Q_j^2 = I$. Their cross products have zero expectation in $(I + \epsilon P_n)/2^n$, so

$F_Q = \epsilon^2 \sum_j \langle Q_j^2 \rangle = \epsilon^2 n$. Independence of the commuting Pauli generators gives all sign patterns; their sums have the stated $n+1$ values. $\square$

For the plotted choice $\epsilon = 1/2$, $\kappa = 3$ and $F_Q = n/4$. These conditioning and score-alphabet statements supplement the anteceded one-clean-qubit sensitivity result. The balanced inputs are especially simple:

$$S_n = I + \epsilon P_n, \qquad D_n = -i\epsilon[H_n, P_n] = L_n. \tag{118}$$

Thus S_n has two Pauli terms and D_n, L_n have n commuting terms. A Clifford stabilizer measurement can read the joint signs, after which their Hamming weight gives the exact $n+1$-valued score. This family is deliberately classically structured; it is not a hardness example. Its role is to refute the possibility that Assumption 2.1 necessarily forces vanishing QFI or an exponentially large readout alphabet.

9.2 Exact Gibbs conditioning obstruction

For an n-spin Hamiltonian with energy span $\Delta E_n = E_{\max}^{(n)} - E_{\min}^{(n)}$, define

$$S_\beta^{(n)} = e^{-\beta(H^{(n)} - E_{\min}^{(n)} I)}. \tag{119}$$

Proposition 9.2 (Rescaling-invariant Gibbs conditioning)**.** *For every scalar $c_0 > 0$,*

$$\kappa(c_0 \rho_\beta^{(n)}) = \kappa(S_\beta^{(n)}) = e^{\beta \Delta E_n}. \tag{120}$$

If $\Delta E_n \geq sn$ and $\kappa \leq n^p$ is required, then

$$\beta \leq \frac{p \log n}{sn}. \tag{121}$$

Conversely, $\sup_n \Delta E_n / n \leq s_+$ *and* $\beta_n = c/n$ *imply* $\kappa \leq e^{cs_+} = O(1)$.

Proof. Positive scalar multiplication does not alter a spectral condition number. The Gibbs eigenvalue ratio is exactly $e^{\beta(E_{\max} - E_{\min})}$. Taking logarithms proves the remaining statements. $\square$

The obstruction is a property of the Gibbs state, not of the chosen balancing scale. For the tested frustrated chain, $\Delta E_{10}/10 = 2.866$. At $n = 10$, $\kappa = 5416.7$ for fixed $\beta = 0.30$ and $\kappa = 4.66 \times 10^{18}$ for $\beta = 1.50$. The inverse-temperature axis is therefore also an exponential compilation-cost axis.

The shrinking window is nonempty but less sensitive. For the perturbation V_n used below,

$$\frac{\operatorname{Tr} V_n^2}{2^n} = 1.49(n-1), \tag{122}$$

so at $\beta = c/n$ the leading high-temperature behavior is

$$F_Q \simeq \beta^2 \frac{\operatorname{Tr} V_n^2}{2^n} = \frac{1.49 c^2 (n-1)}{n^2} = O(n^{-1}). \tag{123}$$

For $c = 1$, exact diagonalization keeps $\kappa \leq 17.56$ through ten spins and gives $0.809 \leq nF_Q \leq 1.202$ over $n = 4, 6, 8, 10$. These finite sizes agree with the leading high-temperature behavior $F_Q = O(n^{-1})$, which would correspond to a linear copy overhead at fixed target precision. We do not prove a uniform nonasymptotic lower bound or an asymptotic sample-complexity theorem for this Gibbs path. Proposition 9.1 separately shows that constant conditioning and extensive sensitivity coexist in another explicit sensor family.

9.3 Frustrated four-spin readout benchmark

Consider

$$\begin{aligned} H_0 = & \sum_{i=1}^{3} (0.9 X_i X_{i+1} + 0.6 Y_i Y_{i+1} + 1.1 Z_i Z_{i+1}) \\ & + 0.35 \sum_{i=1}^{2} Z_i Z_{i+2} + 0.3 \sum_{i=1}^{4} (-1)^{i-1} X_i \\ & + 0.12 \sum_{i=1}^{4} \cos(i\sqrt{2}) Z_i, \end{aligned} \tag{124}$$

$$V = \sum_{i=1}^{3} (X_i Z_{i+1} + 0.7 Z_i X_{i+1}), \tag{125}$$

with

$$\rho_\lambda = \frac{e^{-\beta(H_0 + \lambda V)}}{\operatorname{Tr} e^{-\beta(H_0 + \lambda V)}} \quad (\lambda = 0). \tag{126}$$

The Fréchet derivative of the exponential and the SLD are evaluated by exact dense linear algebra.

An arbitrary product PVM is optimized over an independent Bloch axis on each spin using scrambled Sobol starts followed by L-BFGS-B and Powell polishing. At $\beta = 0.30$,

$$\frac{J_{\text{prod}}}{F_Q} = 0.485497. \tag{127}$$

This is a strong deterministic product baseline, not a proof of its global optimum. The exact dynamic program of Eq. (45) gives

$$\frac{J_7^\star}{F_Q} = 0.983440, \qquad \frac{J_8^\star}{F_Q} = 0.992641. \tag{128}$$

The projectors remain entangled; compression reduces score precision and output alphabet, not the cost of implementing the eigenspaces.

9.4 Partial readout-resource worksheet

At $\beta = 0.30$, shift H_0 by its ground energy and use

$$S = e^{-\beta(H_0 - E_{\min} I)}, \qquad D = \partial_\lambda S - S\, \partial_\lambda \log Z. \tag{129}$$

Exact four-qubit Pauli expansions contain 136, 135, and 136 terms for S, D, L; $\kappa(S) = 20.27$. Under the stated unary SELECT/PREPARE and Ross–Selinger synthesis convention, seven phase bits provide a 128-level register, while the query convention $\lceil 2\pi\alpha_L/\delta \rceil$ gives 123 controlled L queries. These choices give the partial readout-side worksheet in Table 3 [76, 77, 78]. It excludes state preparation, full square-root and Sylvester constants, a composed allocation of η, ξ, and signal-gadget error, routing, and error correction.

TABLE 3. Four-spin partial readout-resource proxy. Counts exclude state preparation, composed precision allocation, error correction, routing, and the hidden square-root and Sylvester implementation constants.

Quantity	Value
$\kappa(S)$	20.27
Pauli terms (S, D, L)	$(136, 135, 136)$
Eight-bin retained QFI	99.264%
Phase-register bits / controlled queries	7 bits/123
Binary-index logical footprint	22 qubits
Unary-accounting logical footprint	150 qubits
T proxy per L-LCU query	52,920
Readout-stage T proxy	6,509,160
SLBB query proxy	$82.4 \times C_{\mathrm{SLBB}}$

At four qubits, direct dense diagonalization and bespoke unitary synthesis are plainly preferable to this generic 6.51×10^6-gate proxy. The table is an upper-bound audit of the scalable block-encoding stack, not a small-instance advantage claim or a surface-code estimate. Its value is diagnostic: it separates physical conditioning, score resolution, LCU normalization, and the hidden Sylvester constant.

The truncation audit reaches a nonzero worst-case exact-PVM Fisher certificate at 23 direct L terms, 48 coefficient-tail-certified terms, or 71 terms per physical input after re-solving the Sylvester equation; 99% certification needs 72, 94, and 114, respectively. The κ-amplified matrix score error in Theorem 6.2 controls this diagnostic; an implemented circuit must additionally certify ξ through Theorem 6.3. Supplemental Fig. S3 archives the curves.

10 Prior work, dequantization, and novelty boundary

The article connects four literatures that usually optimize different outputs: metrological value, finite readout, coherent matrix functions, and projective search geometry. Table 4 records the closest comparison.

10.1 Metrology and measurement synthesis

Helstrom, Holevo, Braunstein–Caves, and Barndorff-Nielsen–Gill establish the SLD, QFI attainability, and adaptive localization needed for local estimation [1, 2, 3, 4]. Modern reviews and applications cover noisy, many-body, and multiparameter sensing [15, 16, 5, 17, 20, 21, 80]. Variational, randomized, shadow, Krylov, and incomplete-data methods estimate or certify F_Q without generally providing the optimizing measurement [22, 23, 24, 25, 26, 27, 28, 29, 30, 31]. Structured SLD constructions remain the appropriate competitors for symmetry-restricted, Gaussian, tensor-network, and master-equation models [33, 34, 35, 36, 37, 38, 39, 40, 41].

The exact residual identity in Proposition 4.1 is a direct completion of the square and should be read as an operational refinement of the standard QFI inequality, not as the source of the general geometry. The no-bad-maxima classification and pair escape are results of the companion Landscape paper [6]; this article supplies the Fisher dictionary and uses them as an exact projective-search certificate under the companion hypotheses.

10.2 Compression and quantization

Once $\nu_{\rho,L}$ is identified, optimal coarse SLD readout is a scalar minimum-mean-square quantization problem. Lloyd–Max conditions, the Panter–Dite–Zador high-rate law, the Bellman/Wang–Song dynamic program, and Wasserstein stability of optimal quantization are established results [61, 62, 66, 67, 63, 64, 69, 70, 65]. Result R1 applies these tools to the state-weighted SLD score measure and does not re-claim the classical quantization results or the underlying law-of-total-variance projection.

A contemporaneous preprint by Sheng fixes an orthogonal classical–quantum record and proves both an exact operator-valued QFI remainder under parameter-independent compression and a Stinespring score-intertwining identity for the lost QFI [71]. Instantiating its fine blocks with the one-dimensional outcomes of a resolved SLD spectral measurement reproduces Eq. (32); its Stinespring theorem also supplies the foundational identity behind Eq. (78). We claim no priority for either identity or the shared projection mechanism. Ref. [71] assumes a physically available monitored record whose conditional quantum outputs are retained. The present application chooses lossy cells of the final SLD spectrum, imposes a uniform delivered compiler contract, separates matrix and actual-instrument error, derives reconstructed-signal control, and composes this interface with the SLD and full-support hardness constructions. The scoped detector contribution combines the sharp arbitrary-bin coefficient and tail-adaptive theorem with an explicit finite-to-dense/atomic-crossover statement.

10.3 Quantum matrix equations and what is hard

Classical Sylvester and Lyapunov algorithms are standard [43, 44]. SLBB construct a quantum block encoding of the solution and establish general BQP power [45]; qubitization and phase-estimation methods supply spectral-processing primitives [54, 55, 56, 57, 72]. Section 6 inserts an operational score-intertwining interface between those matrix/spectral layers and the actual label POVM. Theorem 7.2 shows that hardness survives a full-support, faithful, trace-normalized metrological embedding with con-

Table 4: Closest prior outputs. "Compiler" means a coherent circuit for the physical SLD spectral instrument, not a scalar QFI estimate.

Line of work	Primary output	Generic SLD compiler	Sharp finite readout	Projective geometry	Complexity statement
Quantum estimation [3, 4]	QFI value, attainability, adaptive localization	Existence	No	Optimality conditions	No
Landscape framework [6]	Measured-divergence local-to-global theorem and pair escape	No circuit	No	Benign, exact	No
QFI estimation [23, 26, 27, 28]	Scalar estimates, bounds, or witnesses	No	No	Ansatz dependent or no	No
Coarse sensing [79, 42, 71]	Detector robustness or compressed classical trajectory memory	Fixed/different task	Model specific or exact record loss	No	Memory separation
Scalar quantization [62, 63, 70]	Optimal MSE cells, high-rate laws, exact 1D DP	Classical	General MSE theory	No	No
Quantum Sylvester [45]	Block encoding of a matrix-equation solution	Not specialized	No	No	General BQP power
This work	Sharp score readout, Fisher certificate, operational compiler interface, restricted embedding	**Conditional interface**	**Sharp + tail adaptive**	**Imported theorem + Fisher dictionary**	**Full-support BQP-hard family**

trolled conditioning, zero-score margin, and QFI when the interface is delivered at the stated accuracy. The primitive cost of certifying that interface is left conditional.

10.4 Dequantization boundary

Quantum-inspired linear-algebra algorithms show that block-encoded-looking speedups can disappear when the same data are stored in an ℓ^2 sample-and-query structure and have favorable low-rank or Frobenius-norm parameters [46, 47, 48, 49]. Those algorithms typically assume efficient entry queries, row-norm queries, and sampling from squared row or vector amplitudes. Assumption 2.1 instead grants coherent unitaries whose top-left blocks are S and D; it does not by itself provide the classical samples or entries required by those frameworks.

The distinction gives no universal anti-dequantization theorem. Structured instances can admit both access models, and low-rank promised families should be compared directly with quantum-inspired solvers. The hard family in Sec. 7 is full rank. For bounded-spectrum A of dimension N, $\|A\|_F = \Theta(\sqrt{N})$ generically, so runtimes polynomial in $\|A\|_F$ are not polylogarithmic in N. The parity-coherence family of Proposition 9.1 is unitarily related to the one-clean-qubit metrology probe of Ref. [75]; its probe construction and extensive sensitivity are anteceded. Our use is the explicit SLD, exact score alphabet, conditioning, and balanced-access accounting. It is efficiently classically describable and Clifford measurable and carries no speedup claim. The paper therefore separates three statements: compression can be useful classically, uniform coherent compilation has a conditional quantum implementation path under block access, and worst-case delivery of that coherent interface is BQP-hard unless standard complexity classes collapse.

10.5 Dated novelty assessment

The literature search was updated through August 20, 2026 using recent metrology and quantum-linear-algebra reviews as citation hubs. The claims retained after that audit are: the sharp and tail-adaptive score-compression package with its Wasserstein dense-spectrum bridge; the Fisher use of the cited Landscape geometry; the full-support faithful hardness embedding; and the explicit constant-conditioned extensive-QFI family. This is a dated search conclusion, not an absolute priority guarantee.

11 Discussion and outlook

The central object is the SLD score, and the paper distinguishes three uses of it. Result R1 asks how much of the score spectrum a detector must retain. Result R2 concerns direct search over physical projectors and uses the companion Landscape theorem as an exact geometric certificate, without asserting a convergence rate or noise robustness. Result R3 formulates an operational interface between a matrix approximation and the actual coherent label circuit, then studies the worst-case complexity of delivering that interface. The exact residual identity connects these regimes while their algorithms remain distinct.

11.1 What score compression buys

A model may have exponentially many SLD eigenvectors while the score distribution is concentrated enough that a small alphabet preserves nearly all QFI. Compression does not make the entangled spectral projectors local. It reduces phase precision, classical memory, calibration levels, and estimator complexity once the score measurement is available. The four-spin instance makes the distinction concrete: product readout retains 48.55%, but eight global score cells retain 99.26%.

Theorems 3.1 and 3.3 are directly testable without a quantum-speedup claim. An experiment may estimate the score distribution, choose Lloyd–Max or constrained bins, and compare the measured loss with the exact conditional-variance identity. Corollary 3.5 gives the correct many-level asymptotic statement: an intermediate quantization window can coexist with an exact zero-loss crossover at the finite support size.

11.2 Access, conditioning, and physical regimes

The coherent complexity result assumes explicit block encodings, a uniform score-intertwining contract, and BQP $\neq$ BPP. These assumptions define an output problem with no implied laboratory shortcut. For each sensor family, an end-to-end comparison must count state preparation, derivative access, block-encoding normalization, spectral resolution, circuit-interface certification, and the best specialized classical algorithm under comparable access.

Two examples clarify that boundary. The parity-coherence sensor has constant conditioning, extensive QFI, sparse Pauli access, and an exact logarithmic-size score register; it is scalable and classically structured. The frustrated Gibbs sensor has a nontrivial entangled readout gap, while fixed temperature produces exponential conditioning for an extensive energy span. Its $\beta = c/n$ window has bounded conditioning over the tested finite sizes, with nF_Q remaining of order one through ten spins. The asymptotic sensitivity and copy complexity of that Gibbs path remain open. Together the examples show that usefulness and promised access are compatible, while usefulness alone does not imply quantum advantage.

Dequantization must be assessed instance by instance. Block encoding does not automatically supply ℓ^2 sample-and-query access, and the full-rank hardness family does not have favorable generic Frobenius scaling. Low-rank or classically sampled models may nevertheless admit quantum-inspired solvers. Conversely, Theorem 7.2 establishes only coherent synthesis hardness. In fact, its entire marginal score histogram is independent of the encoded right-hand side: the computational content is isolated in the SLD eigenvectors and their coherent action.

A single natural sensor occupying all three sets—promise-compatible access, nonvanishing metrological value, and no matched efficient classical description—remains open. The parity family occupies the first two sets and is Clifford structured. The hardness family establishes the third property for coherent synthesis through a computational embedding. Their narrower intersection is the appropriate target for a future end-to-end quantum-metrology advantage claim.

11.3 Scope and next theorems

The compression theorem includes pure and rank-deficient probes at SLD-regular operating points. The smooth projective landscape and conditioned compiler do not: as the minimum eigenvalue vanishes, their present κ-dependent statements lose force. A stratified critical-point theorem and support-adaptive coherent solver would extend the geometric and algorithmic branches to canonical pure-state sensors.

Other immediate directions are:

1. **Implementability-constrained quantization.** Determine the extra Fisher distortion imposed by locality, bounded depth, detector symmetries, or restricted entangling layers.

2. **Finite-sample integration.** Combine the compiler error budget with preliminary localization, estimator bias, and confidence intervals in a nonasymptotic resource theorem.

3. **Multiparameter scores.** Replace one scalar SLD by an incompatibility-aware matrix score and quantify the joint cost of noncommuting readouts.

4. **Matched classical baselines.** For each physical access construction, benchmark tensor-network, Krylov, sparse-Pauli, and sample-query solvers against the coherent compiler.

12 Conclusion

The information-bearing output of an optimal quantum measurement can be much smaller than its eigenbasis. We proved sharp and tail-adaptive score-compression bounds, connected finite atomic models to a dense-spectrum quantization limit, and found 99.26% QFI retention with eight bins in a sensor whose best archived heuristic product readout captures less than half. The exact projective residual provides a stopping certificate, while the cited Landscape theorem supplies benign search geometry under its declared hypotheses. At the coherent layer, the score-intertwining theorem gives an operational Fisher-loss and signal-reconstruction budget for any implementation that certifies its uniform defect. Full-support synthesis satisfying that interface remains BQP-hard under restrictive metrological promises; the primitive cost of attaining the interface remains conditional. The parity-coherence family shows that constant conditioning, extensive sensitivity, and logarithmic score memory can coexist. These results provide a theory and benchmark toolkit for separating inexpensive score resolution from difficult coherent compilation.

Acknowledgments

The research workflow used NumPy, SciPy, Matplotlib, and the LaTeX toolchain. No external funding was used for the present work.

Program management. Domingos S. P. Salazar manages the Implementable Quantum Measurement Program and its release guardrails. Program management is recorded separately from research authorship.

Data availability. All data underlying the figures, including raw Monte Carlo records, product-measurement search parameters, and numerical validation summaries, are contained in the private candidate package accompanying this version. The public reproducibility identifier remains unassigned and is a release blocker.

Code availability. The candidate package contains deterministic Python code for the simulations and figures, a rebuild orchestrator, machine-readable numerical tolerances, exact Pauli decompositions for the partial resource worksheet, and the dynamic program used for optimal score binning.

Agent provenance. Maestro v0.1 is the research author. The recorded underlying model is GPT-5.6 Pro; the model snapshot and model-knowledge cutoff are unknown. The literature cutoff is recorded independently in the Ledger dossier.

A Strong concavity, the PL inequality, and the Richardson baseline

This appendix supplies the conditioning statements used in Sec. 5. The iteration is standard Richardson/Jacobi applied to the SLD Sylvester superoperator. Its metrological content comes from combining operator-space contraction with the exact Fisher residual identity proved in Proposition 4.1; the nonconvex projective geometry itself is imported from Ref. [6].

Assume

$$\mu I \preceq \rho \preceq \Lambda I, \qquad \kappa = \Lambda/\mu. \tag{130}$$

Let $H = X - L$. From Eqs. (59) and (58),

$$\Phi(L) - \Phi(X) = \mathrm{Tr}(\rho H^2) = \frac{1}{2}\langle H, \mathcal{S}_\rho(H)\rangle_{\mathrm{HS}}, \tag{131}$$

and

$$\nabla\Phi(X) = -\mathcal{S}_\rho(H). \tag{132}$$

The eigenvalues of $\mathcal{S}_\rho$ lie in $[2\mu, 2\Lambda]$.

Theorem A.1 (Global PL and smoothness bounds)**.** *For every Hermitian X,*

$$4\mu[\Phi(L)-\Phi(X)] \le \|\nabla\Phi(X)\|_2^2 \le 4\Lambda[\Phi(L)-\Phi(X)]. \tag{133}$$

The potential is 2μ-strongly concave and 2Λ-smooth in Hilbert–Schmidt geometry.

Proof. Expand H in an eigenbasis of the positive self-adjoint superoperator $\mathcal{S}_\rho$. Each component with eigenvalue $s \in [2\mu, 2\Lambda]$ contributes $s|h|^2/2$ to the gap and $s^2|h|^2$ to the squared gradient. Their ratio lies in $[4\mu, 4\Lambda]$. □

Theorem A.2 (Optimal constant-step Richardson/Jacobi iteration)**.** *Let*

$$X_{m+1} = X_m + \eta(2\dot\rho - \rho X_m - X_m\rho), \qquad \eta = \frac{1}{\mu+\Lambda}. \tag{134}$$

Then

$$\begin{aligned} &\|X_m - L\|_2 \le r^m\|X_0 - L\|_2, \\ &\Phi(L) - \Phi(X_m) \le r^{2m}[\Phi(L) - \Phi(X_0)], \qquad r = \frac{\kappa-1}{\kappa+1}. \end{aligned} \tag{135}$$

Proof. The error obeys $H_{m+1} = (I - \eta\mathcal{S}_\rho)H_m$. For $s \in [2\mu, 2\Lambda]$, the minimax constant step is $\eta = 2/(2\mu+2\Lambda) = 1/(\mu+\Lambda)$ and the extremal multiplier is $(\Lambda-\mu)/(\Lambda+\mu) = r$. Apply this componentwise to the Hilbert–Schmidt norm and the weighted quadratic gap. □

The continuous flow is

$$\frac{\mathrm{d}X_t}{\mathrm{d}t} = 2\dot\rho - \rho X_t - X_t\rho, \tag{136}$$

with solution from $X_0 = 0$

$$X_t = 2\int_0^t e^{-s\rho}\dot\rho e^{-s\rho}\,\mathrm{d}s \longrightarrow L. \tag{137}$$

Moreover, $\mathrm{d}\Phi(X_t)/\mathrm{d}t = \|\nabla\Phi(X_t)\|_2^2$. The exact bridge $F_Q - J(P) = \mathrm{Tr}[\rho(L_P - L)^2]$ is what turns any such score approximation into a metrological statement.

B Exact score compression and approximate score measurements

This appendix proves the detailed forms of Result R1 and the approximation budget used by the coherent compiler.

B.1 Exact spectral partitions

Let $L = \sum_a \lambda_a\Pi_a$ and define the state-weighted spectral probability measure

$$\nu_{\rho,L}(\Omega) = \mathrm{Tr}[\rho\,\mathbf{1}_\Omega(L)]. \tag{138}$$

Partition the spectrum into disjoint intervals I_b and set

$$B_b = \mathbf{1}_{I_b}(L), \qquad q_b = \mathrm{Tr}(\rho B_b), \qquad \ell_b = \frac{\mathrm{Tr}(\dot\rho B_b)}{q_b}. \tag{139}$$

Because $[B_b, L] = 0$ and $2\dot\rho = \rho L + L\rho$,

$$\ell_b = \frac{\mathrm{Tr}(\rho L B_b)}{q_b} = \mathbb{E}_{\nu_{\rho,L}}[\lambda \mid I_b]. \tag{140}$$

The binning problem is therefore weighted scalar squared-error quantization of $\lambda \sim \nu_{\rho,L}$, with the usual Lloyd–Max conditional-mean representatives [61, 62, 63].

Theorem B.1 (Exact score-compression identity)**.** *The Fisher information $J_{\mathcal{I}} = \sum_b q_b \ell_b^2$ satisfies*

$$F_Q - J_{\mathcal{I}} = \sum_b \mathrm{Tr}[\rho B_b (L-\ell_b)^2] \tag{141}$$

$$= \sum_b q_b \operatorname{Var}_{\nu_{\rho,L}(\cdot|I_b)}(\lambda)$$

$$\le \frac{1}{4}\sum_b q_b \operatorname{diam}(I_b)^2. \tag{142}$$

The factor $1/4$ is sharp.

Proof. The binned score operator $L_{\mathcal{I}} = \sum_b \ell_b B_b$ obeys $\Phi(L_{\mathcal{I}}) = J_{\mathcal{I}}$. Equation (59) gives the first equality. Equation (140) identifies each term with a conditional variance. Popoviciu's inequality bounds a variance supported on an interval of diameter Δ_b by $\Delta_b^2/4$. Equal mass at two endpoints attains equality, so the constant is sharp. □

If every occupied bin has diameter at most δ, then

$$F_Q - J_\delta \le \delta^2/4. \tag{143}$$

If the occupied spectrum has width W, K equal-width bins give $F_Q - J_K \le W^2/(4K^2)$.

Define the state-weighted tail second moment

$$T_R = \int_{|\lambda|>R} \lambda^2\, \nu_{\rho,L}(\mathrm{d}\lambda). \tag{144}$$

Partition $[-R,R]$ into K equal intervals and use two additional tail bins. The central loss is at most R^2/K^2, while the two tail conditional variances sum to no more than T_R. Hence

$$F_Q - J_{K+2} \le T_R + \frac{R^2}{K^2}. \tag{145}$$

This proves the dimension-free tail statement in Result R1.

For a probability measure ν with finite second moment, define

$$D_K(\nu) = \inf_{|C|\le K} \int \operatorname{dist}(\lambda, C)^2\, \nu(\mathrm{d}\lambda). \tag{146}$$

If ν has m atoms, then $D_K(\nu) = 0$ for $K \ge m$. Since every finite-dimensional SLD measure is atomic, the high-rate density law can only describe a joint dense-spectrum and large-K limit.

Lemma B.2 (Wasserstein stability)**.** *For probability measures μ, ν with finite second moments,*

$$\left|\sqrt{D_K(\mu)} - \sqrt{D_K(\nu)}\right| \le W_2(\mu,\nu). \tag{147}$$

Proof. Fix a codebook C with at most K points and any coupling (X,Y) of μ and ν. The distance-to-set function is 1-Lipschitz, so Minkowski's inequality gives

$$\|\operatorname{dist}(X,C)\|_{L^2} \le \|\operatorname{dist}(Y,C)\|_{L^2} + \|X-Y\|_{L^2}. \tag{148}$$

Take the infimum first over couplings and then over C to obtain $\sqrt{D_K(\mu)} \le \sqrt{D_K(\nu)} + W_2(\mu,\nu)$. Interchanging μ and ν proves Eq. (147). □

Now let ν_n be finite atomic score measures with support cardinalities $m_n := \#\operatorname{supp}\nu_n \to \infty$ and assume $W_2(\nu_n,\nu) \to 0$, where $\nu = f(\lambda)\mathrm{d}\lambda$ has a compactly supported density continuous and positive on the interior of its support. The rigorous one-dimensional squared-error theorem of Graf and Luschgy, Theorem 6.2, gives

$$K^2 D_K(\nu) \longrightarrow C_f := \frac{1}{12}\left(\int f(\lambda)^{1/3}\,\mathrm{d}\lambda\right)^3. \tag{149}$$

For any sequence $K_n \to \infty$ with $K_n < m_n$ and $K_n W_2(\nu_n,\nu) \to 0$, Eq. (147) implies

$$\left|K_n\sqrt{D_{K_n}(\nu_n)} - K_n\sqrt{D_{K_n}(\nu)}\right| \to 0. \tag{150}$$

Combining this with Eq. (149) and the exact metrological identity yields

$$K_n^2\big(F_Q^{(n)} - J_{K_n}^{\star,(n)}\big) \longrightarrow C_f. \tag{151}$$

At $K \ge m_n$, the finite atomic distortion is exactly zero, while it is positive for $K < m_n$ because every atom has positive mass and at least one support point lies outside any smaller codebook. This proves Corollary 3.5 and cleanly separates the intermediate high-rate window from the terminal finite-support crossover. The classical law is imported from Refs. [66, 67, 68, 63, 64]; the constant-one root-distortion Wasserstein inequality is directly anteceded by Ref. [65].

For sorted finite eigenvalues with weights $w_a = \mathrm{Tr}(\rho\Pi_a)$, the exact cost of a contiguous interval $i \le a < j$ is

$$C(i,j) = \sum_{a=i}^{j-1} w_a\lambda_a^2 - \frac{\left(\sum_{a=i}^{j-1} w_a\lambda_a\right)^2}{\sum_{a=i}^{j-1} w_a}. \tag{152}$$

The Bellman recursion $D(k,j) = \min_{i<j}\{D(k-1,i) + C(i,j)\}$ finds the exact optimal contiguous K-bin partition in $O(Kd^2)$ time [69, 70].

B.2 Approximate block-encoded score

Theorem B.3 (Exact approximate-operator PVM)**.** *Suppose $\mu I \preceq \rho \preceq \Lambda I$, $\kappa = \Lambda/\mu$, and $\widetilde{L} = \widetilde{L}^\dagger$ satisfies*

$$\|\widetilde{L} - L\|_\infty \le \eta. \tag{153}$$

Let (B_b) be spectral bins of $\widetilde{L}$ of diameter at most δ. Then

$$F_Q - J_{\delta,\widetilde{L}} \le \min\left\{(\kappa+1)^2\eta^2 + \frac{(\delta+2\kappa\eta)^2}{4},\right.$$

$$\left.\big[\delta + (\kappa+1)\eta\big]^2\right\}. \tag{154}$$

For the rank-one eigenbasis of $\widetilde{L}$ ($\delta = 0$), the second branch gives $(\kappa+1)^2\eta^2$.

Proof. Let $\widetilde{L}|j\rangle = \widetilde{\lambda}_j|j\rangle$ and $q_j = \langle j|\rho|j\rangle$. The exact classical score generated by this basis satisfies

$$\ell_j - \widetilde{\lambda}_j = \frac{\langle j|[\rho(L-\widetilde{L}) + (L-\widetilde{L})\rho]|j\rangle}{2q_j}, \qquad (155)$$

so $|\ell_j - \widetilde{\lambda}_j| \le \kappa\eta$. The induced rank-one score operator L_P therefore obeys $\|L_P - L\|_\infty \le (\kappa+1)\eta$, and Proposition 4.1 gives $F_Q - J(P) \le (\kappa+1)^2\eta^2$. Within one approximate spectral bin, the exact classical scores have range at most $\delta + 2\kappa\eta$. The exact Fisher chain rule between the refined PVM and its coarse graining, followed by Popoviciu's inequality, gives the first branch.

For the direct branch, let $L_{\mathcal{B}} = \sum_b \bar{\ell}_b B_b$ be the coarse score operator. For every $\widetilde{L}$ eigenvector in bin b, $|\bar{\ell}_b - \widetilde{\lambda}_j| \le \delta + \kappa\eta$, so $\|L_{\mathcal{B}} - L\|_\infty \le \delta + (\kappa+1)\eta$. The exact complete-square identity for the coarse PVM then gives $F_Q - J_{\delta,\widetilde{L}} \le [\delta + (\kappa+1)\eta]^2$. □

If a block encoding approximates L/x with operator error ϵ, then $\eta \le x\epsilon$. This statement controls the matrix approximation and the exact spectral PVM analyzed above. The actual coherent circuit has the separate uniform score-intertwining defect ξ of Eq. (24). A failure probability contributes to ξ only after every failure label receives a bounded score and the primitive guarantee is made uniform over inputs; amplification alone does not supply that interface.

C Quantum score compiler and resource accounting

This appendix documents the matrix layer, the operational score interface used in Result R3, and the partial resource convention audited in Result R4.

Definition C.1 (Balanced block-encoding input)**.** *The input is an n-qubit one-parameter model supplied through block encodings of*

$$S = c\rho, \qquad D = c\dot{\rho}, \qquad (156)$$

with common known scale $c > 0$, spectral promise

$$\mu I \preceq S \preceq \Lambda I, \qquad \kappa = \Lambda/\mu = \mathrm{poly}(n), \qquad (157)$$

and block-encoding normalization α for D/Λ. The accelerated positive-matrix routine also receives block encodings of $\sqrt{S/(2\Lambda)}$.

The common scale is essential: the SLD equation is invariant under $(\rho, \dot{\rho}) \mapsto (c\rho, c\dot{\rho})$, whereas a normalized density-matrix block encoding can hide an exponential normalization factor.

Algorithm 6.1 specifies the complete compiler interface. In the matrix layer it sets $A = B = S/(2\Lambda)$ and the Sylvester right-hand side to D/Λ, then invokes the quantum linear-matrix-equation circuit of Ref. [45] to obtain a block encoding of $\widetilde{L}/x$. Equation (154) converts matrix and bin-width errors into a Fisher bound for the exact spectral PVM of $\widetilde{L}$. Theorem 6.3 converts the actual circuit's separately certified defect ξ into the implemented-POVM bound.

For $A = B = S/(2\Lambda)$, the Kronecker-sum coefficient has spectrum in $[1/\kappa, 1]$. The positive-matrix case of Ref. [45] uses

$$Q_{\mathrm{Syl}} = O\left(\sqrt{\kappa}\log\frac{\kappa d}{\epsilon}\right) \qquad (158)$$

coefficient-oracle queries and returns normalization

$$x = O\left(\alpha\kappa\log\frac{\kappa d}{\epsilon}\right), \qquad (159)$$

up to the constants and mild logarithmic factors specified there. Qubitization and phase estimation at physical resolution δ require $O[(x/\delta)\log(1/\zeta)]$ uses of the L/x block encoding [54, 55, 56, 57]. Thus

$$Q_{\mathrm{matrix+spectral}} = \widetilde{O}\left(\frac{\alpha\kappa^{3/2}}{\delta}\right), \qquad (160)$$

with logarithmic dependence on $d = 2^n$, $1/\epsilon$, and the primitive's declared failure target. This is an end-to-end query bound only when the primitive proves that these choices yield the uniform ξ required by Eq. (74), including boundary, leakage, failure-score, and representative-range effects. Without square-root access, the analogous conditional normal-matrix expression is $\widetilde{O}(\alpha\kappa^2/\delta)$.

Table 5 is also archived as `metadata/oracle-interface.json`. It is an audit of the reduction and its promises, not a claim that a particular phase-estimation circuit already proves the primitive-to-ξ implication.

For the four-spin worksheet, every balanced operator is decomposed exactly as $O = \sum_p c_p P_p$ over Pauli strings. The LCU normalization is $\alpha_O = \sum_p |c_p|$. Under the explicitly stated unary SELECT/PREPARE convention, one M-term query is charged $4(M-1)$ synthesized rotations. Dividing target block error 10^{-6} evenly over those rotations and using the Ross–Selinger synthesis proxy gives the table in Sec. 9 [76, 77, 78]. These counts form a partial readout proxy. They exclude state preparation, complete square-root and Sylvester constants, composed allocation of η, ξ, and signal-gadget error, routing, and error correction.

The archived truncation audit separates three notions. First, direct truncation of the exactly known L is evaluated in operator norm. Second, the Pauli coefficient tail $\sum_{p\notin\mathcal{K}} |c_p|$ gives a basis-independent sufficient bound on that operator error. Third, the physical-input audit truncates S and D, resolves the perturbed Sylvester equation, and measures the induced $\|\widetilde{L} - L\|_\infty$. For the benchmark, the nonzero-information threshold $\sqrt{F_Q}/(\kappa+1) = 0.02425$ is crossed at 23, 48, and 71 retained terms in these three diagnostics, while a 99% rank-one certificate requires 72, 94, and 114, respectively. Supplemental Fig. S3 shows the complete curves. The disparity demonstrates why raw

Table 5: Oracle and interface audit for the full-support hardness reduction. Every row is a reduction input, construction, or verified consequence. The spectral primitive's delivery of the uniform ξ contract is deliberately isolated as an unproved implementation obligation rather than hidden in the query expression.

Item	Supplied or constructed object	Cost, error, and use
QLS access	Block encoding of Hermitian H and state preparation $U_b\|0\rangle = \|b\rangle$; normal equations construct $A = H^2$ and $\|b'\rangle \propto H\|b\rangle$.	Polynomial overhead in κ_H; $\kappa_A \le \kappa_H^2$.
Metrological input	Direct sums and linear combinations construct block encodings of S and T in Eqs. (164)–(165), with common scale and known normalization.	Polynomial overhead; $S \succeq aI$ and $\kappa(\rho_0) \le 2\kappa_A - 1$.
Square-root access	Quantum singular-value transformation of the positive block encoding of $S/(1-a)$.	Polynomial degree in κ_A and logarithmic in inverse error; this is supplied to the accelerated Sylvester routine.
Matrix solve	Quantum linear-matrix-equation circuit returns a block encoding of $\widetilde{L}/x$.	Matrix error $\eta = \\|\widetilde{L} - L\\|_\infty$ is charged explicitly; normalization x is retained.
Score representation	An initialized, parameter-independent isometry V, exhaustive labels, and bounded label-score observable C.	The delivered interface must certify $\xi = \\|CV - V\widetilde{L}\\|_\infty$, including ordinary, boundary, leakage, clipping, and failure labels.
Signal gadget	A label-controlled block K at scale 2 with $\\|K - 2C\\|_\infty \le \chi$.	Exact uncomputation yields $2L_c = V^\dagger K V$ and $\\|L_c - L\\|_\infty \le \eta + \xi + \chi/2$.
Recovery	Apply the reconstructed block to $\|2, 0\rangle$ and postselect the signal/computational branch.	If $\tau := \eta + \xi + \chi/2 < 1/(2\kappa_A)$, success is at least $(1/\kappa_A - 2\tau)^2$ and normalized error is at most $4\kappa_A\tau$.
Precision composition	Require $\eta + \xi + \chi/2 \le \epsilon_{\mathrm{QLS}}/(4\kappa_A)$.	Gives normalized QLS error at most ϵ_{QLS} and, for $\epsilon_{\mathrm{QLS}} \le 1$, success at least $1/(4\kappa_A^2)$ before amplification.
Output boundary	Coherent action on chosen inputs, including signal reconstruction.	No hardness claim is made for the marginal score histogram, ordinary samples, or stronger classical sample/query access.

Pauli sparsity and conditioned score accuracy must not be conflated.

Remark C.2 (Local parameter dependence)**.** *The optimal SLD measurement depends on the unknown operating point. In local estimation, use $o(N)$ copies for coarse localization, compile the SLD at the preliminary estimate, and measure the remaining copies. Under smoothness, the localization error vanishes and the asymptotic variance approaches $(NF_Q)^{-1}$ [59].*

D BQP-hardness of coherent SLD-measurement synthesis

This appendix gives the access reduction and error accounting for Result R3. The output is an actual parameter-independent initialized isometry V, exhaustive labels with bounded score operator C, and a uniform score-intertwining defect ξ. This coherent contract controls chosen inputs and is stronger than a state-averaged classical score sample. A particular phase-estimation circuit belongs to the task only after it certifies the declared interface.

D.1 Positive QLS remains BQP-hard

The standard quantum linear-systems problem is BQP-hard under sparse or block-encoding access [73, 74]. Restricting the coefficient matrix to be positive definite changes only polynomial conditioning.

Lemma D.1 (Reduction to positive QLS)**.** *Let $H = H^\dagger$ be invertible, $\|H\| \le 1$, and $\|H^{-1}\| \le \kappa_H$. Set*

$$A = H^2, \qquad |b'\rangle = \frac{H|b\rangle}{\|Hb\|}. \tag{161}$$

Then $A > 0$, $\kappa_A := \kappa(A) \le \kappa_H^2$, and

$$\frac{A^{-1}|b'\rangle}{\|A^{-1}b'\|} = \frac{H^{-1}|b\rangle}{\|H^{-1}b\|}. \tag{162}$$

A block encoding of A and a preparation of $|b'\rangle$ require polynomial overhead in κ_H.

Proof. Equation (162) follows from $H^{-2}H = H^{-1}$. A block encoding of H^2 follows by block-encoding multiplication. Applying the encoding of H to $|b\rangle$ succeeds with amplitude $\|Hb\| \ge 1/\kappa_H$, so amplitude amplification prepares $|b'\rangle$ with polynomial overhead. □

D.2 Full-support faithful metrology embedding

Let $A > 0$ have spectrum in $[1/\kappa_A, 1]$, let $|b\rangle$ be normalized, and let $U_b|0\rangle = |b\rangle$. For compactness write $\kappa = \kappa_A$ within this subsection and define

$$a = \frac{1}{2\kappa}, \qquad \gamma = \frac{a}{2}, \tag{163}$$

and, on $\mathcal{H}_1 \oplus \mathcal{H}_2$,

$$S = \begin{pmatrix} A - aI & 0 \\ 0 & aI \end{pmatrix}, \tag{164}$$

$$T = \gamma \begin{pmatrix} 0 & U_b \\ U_b^\dagger & 0 \end{pmatrix}, \tag{165}$$

$$\rho_\theta = \frac{S + \theta T}{Z}, \qquad Z = \operatorname{Tr} S = \operatorname{Tr} A. \tag{166}$$

Because $\operatorname{Tr} T = 0$, ρ_θ is trace one whenever it is positive.

Lemma D.2 (Faithfulness and conditioning)**.** *For every $|\theta| \le 1$, $\rho_\theta > 0$ and*

$$aI \preceq S \preceq (1-a)I, \qquad \kappa(\rho_0) \le 2\kappa - 1. \tag{167}$$

Proof. The first block $A - aI$ has spectrum in $[a, 1-a]$ and the second block equals aI, so $S \succeq aI$. Moreover, the Hermitian off-diagonal unitary block in Eq. (165) has norm one, and therefore $\|T\| = \gamma = a/2$. Weyl's inequality yields

$$S + \theta T \succeq (a - |\theta|\gamma)I = a\left(1 - \frac{|\theta|}{2}\right) I \succeq \frac{a}{2} I > 0 \tag{168}$$

for $|\theta| \le 1$. This proves positivity throughout the stated parameter interval and Eq. (167). It also explains the limiting numerical margin $\lambda_{\min}(S \pm T)/a = 1/2$. □

Normalization cancels from the SLD equation, so $SL + LS = 2T$. The unique solution is

$$L = \begin{pmatrix} 0 & aA^{-1}U_b \\ aU_b^\dagger A^{-1} & 0 \end{pmatrix}. \tag{169}$$

Indeed, its upper-right block X obeys $(A - aI)X + XaI = AX = aU_b$. If $A|v_i\rangle = \lambda_i |v_i\rangle$, then

$$|\pm, i\rangle = \frac{|1, v_i\rangle \pm |2, U_b^\dagger v_i\rangle}{\sqrt{2}}, \qquad L|\pm, i\rangle = \pm \frac{a}{\lambda_i} |\pm, i\rangle. \tag{170}$$

Consequently,

$$\operatorname{spec}(L) = \left\{ \pm \frac{a}{\lambda_i(A)} \right\}_{i=1}^{N}, \qquad a \le |\lambda(L)| \le \frac{1}{2}. \tag{171}$$

There is no zero SLD sector.

The QFI is

$$F_Q = \frac{\operatorname{Tr}(SL^2)}{\operatorname{Tr} S} = \frac{a^2 \operatorname{Tr}(A^{-1})}{\operatorname{Tr} A}. \tag{172}$$

Since $N/\kappa \le \operatorname{Tr} A \le N$ and $N \le \operatorname{Tr} A^{-1} \le \kappa N$,

$$\frac{1}{4\kappa^2} \le F_Q \le \frac{1}{4}. \tag{173}$$

Thus the metrological weight is inverse polynomial under the promised conditioning.

D.3 Coherent recovery of the QLS solution

Let V denote the actual initialized isometry and let C assign a bounded score to every ordinary, boundary, leakage, and failure label. Scores are clipped to $[-1/2, 1/2]$, with the resulting discrepancy charged in ξ. Introduce a signal qubit and a label-controlled gadget whose actual upper-left label block K satisfies

$$\|K - 2C\|_\infty \le \chi. \tag{174}$$

Conjugating by the same actual circuit and its inverse gives the exact initialized-ancilla signal block

$$2L_c = V^\dagger K V. \tag{175}$$

Corollary 6.4 yields

$$\tau := \|L_c - L\|_\infty \le \eta + \xi + \frac{\chi}{2}. \tag{176}$$

Exact reversal proves Eq. (175); the score-intertwining contract supplies proximity to L.

In the exact limit $L_c = L$,

$$L|2, 0\rangle = a|1\rangle\, A^{-1} U_b |0\rangle = a|1\rangle\, A^{-1} |b\rangle. \tag{177}$$

The exact postselection probability is

$$p_{\mathrm{app}} = 4a^2 \|A^{-1} b\|^2 \ge \frac{1}{\kappa_A^2}, \tag{178}$$

The implemented postselection probability obeys

$$p_{\mathrm{app}}^{\mathrm{impl}} \ge (1/\kappa_A - 2\tau)^2. \tag{179}$$

For $\tau < 1/(2\kappa_A)$ the implemented output is nonzero. The normalization inequality gives vector error at most $4\kappa_A \tau$, so

$$\eta + \xi + \frac{\chi}{2} \le \frac{\epsilon_{\mathrm{QLS}}}{4\kappa_A} \tag{180}$$

suffices for normalized error at most ϵ_{QLS}. For $\epsilon_{\mathrm{QLS}} \le 1$, Eq. (179) remains at least $1/(4\kappa_A^2)$, and amplitude amplification has polynomial cost.

Composing with the preceding normal-equations lemma gives $\kappa_A \le \kappa_H^2$. In terms of the original Hermitian QLS condition number,

$$\kappa(\rho_0) \le 2\kappa_H^2 - 1, \qquad g_0(L) \ge \frac{1}{2\kappa_H^2},$$
$$F_Q \ge \frac{1}{4\kappa_H^4}, \qquad p_{\mathrm{app}} \ge \frac{1}{\kappa_H^4}. \tag{181}$$

Combining these bounds with positive-QLS hardness proves Theorem 7.2.

D.4 Access construction and output boundary

Block encodings of S and T follow by direct sums and linear combinations of a block encoding of A, the identity, and U_b. Because the spectrum of $S/(1-a)$ lies in $[a/(1-a), 1]$, quantum singular-value transformation constructs an inverse-polynomially accurate block encoding of the positive square root required by the accelerated Sylvester routine with degree polynomial in κ and logarithmic in the inverse error [56]. If $2N$ is not the desired register dimension, pad both blocks by uncoupled copies of aI and pad T by zero; this does not affect the computational sector.

The reduction proves hardness of the compiled coherent map on chosen inputs. It makes no hardness claim for ordinary score samples from ρ_0. Equation (170) gives

$$\mathrm{Tr}(\rho_0 |\pm, i\rangle\langle\pm, i|) = \frac{\lambda_i(A)}{2\,\mathrm{Tr}\,A}, \tag{182}$$

which has full support and is independent of $|b\rangle$. Thus the marginal score histogram provably erases the QLS right-hand side even though the coherent eigenvectors retain it. The reduction locates the computational content in the implemented spectral basis and its action on $|2,0\rangle$. Result R3 is therefore stated for uniform coherent synthesis.

E Numerical protocol and independent gates

This appendix documents the numerical and resource components of Result R4. All data were generated with Python, NumPy, SciPy, and Matplotlib using master seed 20260818. Dense diagonalization validates finite-dimensional identities; no dense classical runtime is compared with abstract quantum query complexity.

E.1 Projective landscape and residual identity

The explicit saddle uses

$$\rho = I/3, \qquad \dot\rho = \begin{pmatrix} 0.1 & 0.2 & 0 \\ 0.2 & 0.1 & 0 \\ 0 & 0 & -0.2 \end{pmatrix}. \tag{183}$$

At the computational PVM, the scores are $(0.3, 0.3, -0.6)$, $J = 0.18$, and $F_Q = 0.42$. The equal-score residual has off-diagonal entry 0.2, so the inherited pair-rotation formula predicts curvature 1.92. A central finite difference gives 1.9199997; an inter-block direction has curvature -1.0800005.

The exact residual identity was evaluated for 600 PVMs in $d = 16$ at state condition number 8. Geodesic perturbations of the exact SLD eigenbasis covered relative gaps from 10^{-8} to order one and were supplemented by Haar-random PVMs. The maximum absolute discrepancy was 8.59×10^{-18}.

E.2 Compression, finite resolution, and dense spectra

For finite resolution, 40 random $d = 32$, $\kappa = 8$ models were spectrally binned over 13 requested resolutions. The maximum $(F_Q - J_\delta)/(\delta^2/4)$ was 0.366541, with no violation beyond the archived floating-point allowance. A separate ensemble used 20 models at each $d \in \{8, 16, 32, 64\}$ and exact dynamic programming for target fractions $90\%, 95\%, 98\%, 99\%$. At 99%, the exact median bin counts were $7, 10, 12, 14$ and the instance-specific tail theorem guaranteed $25.5, 28, 30, 31.5$. The corresponding finite-range log fits have $R^2 = 0.989$ and 0.988.

For the constructive tail gate, the four-spin model at $\beta = 0.30$ was partitioned exactly as in Theorem 3.3 for $R \in \{0.5, 1, 1.5, 2\}$ and $K \in \{4, 8\}$. The maximum loss-to-budget ratio was 0.323037.

The dense-spectrum gate uses $\rho_m = I/m$ and uniform midpoint scores on $[-1, 1]$ for $m = 64, 128, 256$. For every archived divisor K of m, the dynamic program agrees with

$$D_K = \frac{1}{3K^2} - \frac{1}{3m^2}. \tag{184}$$

The maximum intermediate-window relative error from the limiting constant 1/3 is 0.015625, and $D_m = 0$ exactly.

E.3 Standard score iteration

For the Richardson/Jacobi diagnostic, we generated 20 random $d = 32$ models at each $\kappa \in \{2, 4, 8, 16\}$. Density eigenvalues were geometrically spaced and randomly conjugated. A random traceless derivative was rescaled to $\|\rho^{-1/2}\dot\rho\rho^{-1/2}\|_\infty = 0.3$. The exact step $1/(\mu+\Lambda)$ was used without fitted rates. At $\kappa = 16$, the median normalized potential gap after 90 iterations is 7.815×10^{-13}.

E.4 Full-support hardness family

We tested 123 positive QLS instances over dimensions $4, 8, 16$: 120 interior promised instances with $\kappa = 2, 4, 8, 16, 32$ and three near-identity instances with $\kappa = 1.05$. The interior spectra have $\lambda_{\max}(A) < 1$, so neither the score-margin gate nor the scaled-QFI gate is an endpoint identity. For each instance we construct S, T, L from Eqs. (85)–(90), solve the Sylvester equation numerically, apply L to $|2,0\rangle$, and compare with the normalized $A^{-1}|b\rangle$. The largest relative Sylvester residual is 4.494×10^{-15}, the largest relative SLD error is 4.203×10^{-15}, and the minimum fidelity is 0.9999999999999996. The minimum scaled application success is 1.047458, the minimum scaled QFI is 1.060359, the minimum zero-score margin is $1.005487a$, and the minimum positivity margin is $0.500000a$. The near-identity subset drives the scaled QFI ratio toward its AM–HM lower bound, with archived minimum 1.060359. Its minimum score-margin ratio is 1.010101; the slightly smaller global value 1.005487 comes from an interior-spectrum instance. Every numerical SLD has full nonzero support. At fixed A, a second independent right-hand side changes the complete score histogram by at most 3.220×10^{-15}.

E.5 Promise-compatible sensor and Gibbs benchmark

For the parity-coherence family, the archived sequence $n = 2, 4, 8, 16, 32, 64, 128$ evaluates the analytic formulas $\kappa = 3$, $F_Q = n/4$, and $n + 1$ exact scores. At $n = 128$, $F_Q = 32$ and the exact score label needs eight bits.

The frustrated four-spin benchmark is defined by

$$\begin{aligned} H_0 &= \sum_{i=1}^{n-1}(0.9X_iX_{i+1} + 0.6Y_iY_{i+1} + 1.1Z_iZ_{i+1}) \\ &\quad + 0.35\sum_{i=1}^{n-2} Z_iZ_{i+2} + 0.3\sum_{i=1}^{n}(-1)^{i-1}X_i \\ &\quad + 0.12\sum_{i=1}^{n}\cos(i\sqrt{2})Z_i, \\ V &= \sum_{i=1}^{n-1}(X_iZ_{i+1} + 0.7Z_iX_{i+1}), \end{aligned} \tag{185}$$

with $\rho_\lambda \propto e^{-\beta(H_0+\lambda V)}$ at $\lambda = 0$. The Fréchet derivative is evaluated in the energy basis. The product-PVM baseline optimizes an independent Bloch axis on every spin using scrambled Sobol starts, L-BFGS-B, and Powell polishing. At $\beta = 0.30$, it gives $J_{\mathrm{prod}}/F_Q = 0.485497$, while optimal seven- and eight-bin readouts retain 0.983440 and 0.992641.

For $n = 2, 4, 6, 8, 10$, the exact identity $\kappa = e^{\beta\Delta E_n}$ holds to relative error below 1.4×10^{-16}. At $n = 10$, $\kappa = 5.42 \times 10^3$ for fixed $\beta = 0.30$ and 4.66×10^{18} for fixed $\beta = 1.50$. At $\beta = 1/n$, the condition number remains at most 17.56 through $n = 10$, while $0.809 \le nF_Q \le 1.202$ for $n = 4, 6, 8, 10$.

The Pauli audit orders coefficients by magnitude. Direct operator-norm truncation of L reaches the nonzero/99% information thresholds after 23/72 terms; the coefficient-tail sufficient bound requires 48/94. Truncating both physical inputs and resolving the perturbed Sylvester equation requires 71/114 terms per input.

Independent numerical gates. The executable validator contains 34 checks grouped into 12 families:

G1. exact projective geometry and residual identity;

G2. Richardson conditioning diagnostic;

G3. sharp finite spectral resolution;

G4. random optimal score quantization;

G5. constructive tail-adaptive compression;

G6. dense-spectrum high-rate window and atomic crossover;

G7. full-support faithful QLS-to-SLD embedding, including application success and QFI;

G8. frustrated thermal-sensor readout;

G9. resource and Pauli-truncation audit;

G10. fixed-temperature Gibbs conditioning obstruction;

G11. shrinking-temperature Gibbs window; and

G12. constant-conditioned extensive-QFI parity sensor.

The file `validate.py` exits nonzero if any threshold fails.

References

[1] Carl W. Helstrom. *Quantum Detection and Estimation Theory.* Academic Press, New York, 1976.

[2] Alexander S. Holevo. *Probabilistic and Statistical Aspects of Quantum Theory.* Edizioni della Normale, Pisa, 2 edition, 2011.

[3] Samuel L. Braunstein and Carlton M. Caves. Statistical distance and the geometry of quantum states. *Phys. Rev. Lett.*, 72:3439–3443, 1994.

[4] O. E. Barndorff-Nielsen and R. D. Gill. Fisher information in quantum statistics. *J. Phys. A: Math. Gen.*, 33:4481–4490, 2000.

[5] Matteo G. A. Paris. Quantum estimation for quantum technology. *Int. J. Quantum Inf.*, 7:125–137, 2009.

[6] Domingos S. P. Salazar. Benign projective landscapes for measured quantum divergences. *Benign Projective Landscapes for Measured Quantum Divergences*, public preprint v005, 16 August 2026, GitHub commit 2192529, 2026.

[7] Jarrod R. McClean, Sergio Boixo, Vadim N. Smelyanskiy, Ryan Babbush, and Hartmut Neven. Barren plateaus in quantum neural network training landscapes. *Nat. Commun.*, 9:4812, 2018.

[8] M. Cerezo, Akira Sone, Tyler Volkoff, Lukasz Cincio, and Patrick J. Coles. Cost function dependent barren plateaus in shallow parametrized quantum circuits. *Nat. Commun.*, 12:1791, 2021.

[9] Samson Wang, Enrico Fontana, M. Cerezo, Kunal Sharma, Akira Sone, Lukasz Cincio, and Patrick J. Coles. Noise-induced barren plateaus in variational quantum algorithms. *Nat. Commun.*, 12:6961, 2021.

[10] Michael Ragone, Bojko N. Bakalov, Frédéric Sauvage, Alexander F. Kemper, Carlos Ortiz Marrero, Martín Larocca, and M. Cerezo. A lie algebraic theory of barren plateaus for deep parameterized quantum circuits. *Nat. Commun.*, 15:7172, 2024.

[11] Martín Larocca, Supanut Thanasilp, Samson Wang, Kunal Sharma, Jacob Biamonte, Patrick J. Coles, Lukasz Cincio, Jarrod R. McClean, Zoë Holmes, and M. Cerezo. Barren plateaus in variational quantum computing. *Nat. Rev. Phys.*, 7:174–189, 2025.

[12] M. Cerezo, Martin Larocca, Diego García-Martín, N. L. Diaz, Paolo Braccia, Enrico Fontana, Manuel S. Rudolph, Pablo Bermejo, Aroosa Ijaz, Supanut Thanasilp, Eric R. Anschuetz, Zoë Holmes, et al. Does provable absence of barren plateaus imply classical simulability? *Nat. Commun.*, 16:7907, 2025.

[13] Ryan Babbush, Robbie King, Sergio Boixo, William Huggins, Tanuj Khattar, Guang Hao Low, Jarrod R. McClean, Thomas O'Brien, and Nicholas C. Rubin. Grand challenge of quantum applications. *PRX Quantum*, 7:020101, 2026.

[14] Vittorio Giovannetti, Seth Lloyd, and Lorenzo Maccone. Quantum metrology. *Phys. Rev. Lett.*, 96:010401, 2006.

[15] Vittorio Giovannetti, Seth Lloyd, and Lorenzo Maccone. Advances in quantum metrology. *Nat. Photonics*, 5:222–229, 2011.

[16] Géza Tóth and Iagoba Apellaniz. Quantum metrology from a quantum information science perspective. *J. Phys. A: Math. Theor.*, 47:424006, 2014.

[17] Jasminder S. Sidhu and Pieter Kok. Geometric perspective on quantum parameter estimation. *AVS Quantum Sci.*, 2:014701, 2020.

[18] C. L. Degen, F. Reinhard, and P. Cappellaro. Quantum sensing. *Rev. Mod. Phys.*, 89:035002, 2017.

[19] Luca Pezzè, Augusto Smerzi, Markus K. Oberthaler, Roman Schmied, and Philipp Treutlein. Quantum metrology with nonclassical states of atomic ensembles. *Rev. Mod. Phys.*, 90:035005, 2018.

[20] Jing Liu, Haidong Yuan, Xiao-Ming Lu, and Xiaoguang Wang. Quantum fisher information matrix and multiparameter estimation. *J. Phys. A: Math. Theor.*, 53:023001, 2020.

[21] Victor Montenegro, Chiranjib Mukhopadhyay, Rozhin Yousefjani, Saubhik Sarkar, Utkarsh Mishra, Matteo G. A. Paris, and Abolfazl Bayat. Review: Quantum metrology and sensing with many-body systems. *Phys. Rep.*, 1134:1–62, 2025.

[22] Kok Chuan Tan and Tyler Volkoff. Variational quantum algorithms to estimate rank, quantum entropies, fidelity, and fisher information via purity minimization. *Phys. Rev. Research*, 3:033251, 2021.

[23] Jacob L. Beckey, M. Cerezo, Akira Sone, and Patrick J. Coles. Variational quantum algorithm for estimating the quantum fisher information. *Phys. Rev. Research*, 4:013083, 2022.

[24] Julien Gacon, Christa Zoufal, Giuseppe Carleo, and Stefan Woerner. Simultaneous perturbation stochastic approximation of the quantum fisher information. *Quantum*, 5:567, 2021.

[25] Mourad Halla. Estimation of quantum fisher information via stein's identity in variational quantum algorithms. *Quantum*, 9:1798, 2025.

[26] Aniket Rath, Cyril Branciard, Anna Minguzzi, and Benoit Vermersch. Quantum fisher information from randomized measurements. *Phys. Rev. Lett.*, 127:260501, 2021.

[27] Vittorio Vitale, Aniket Rath, Petar Jurcevic, Andreas Elben, Cyril Branciard, and Benoit Vermersch. Robust estimation of the quantum fisher information on a quantum processor. *PRX Quantum*, 5:030338, 2024.

[28] Da-Jian Zhang and D. M. Tong. Krylov shadow tomography: Efficient estimation of quantum fisher information. *Phys. Rev. Lett.*, 134:110802, 2025.

[29] Guillem Müller-Rigat, Anubhav Kumar Srivastava, Stanisław Kurdziałek, Grzegorz Rajchel-Mieldzioć, Maciej Lewenstein, and Irénée Frérot. Certifying the quantum fisher information from a given set of mean values: A semidefinite programming approach. *Quantum*, 7:1152, 2023.

[30] Iagoba Apellaniz, Matthias Kleinmann, Otfried Gühne, and Géza Tóth. Optimal witnessing of the quantum fisher information with few measurements. *Phys. Rev. A*, 95:032330, 2017.

[31] Rakesh Saini, Jukka Kiukas, Daniel Burgarth, and Alexei Gilchrist. Fisher information of complete quantum measurements. *Phys. Rev. A*, 2026. Accepted 27 July 2026.

[32] Sisi Zhou and Senrui Chen. Randomized measurements for multiparameter quantum metrology. *PRX Quantum*, 7:010314, 2026.

[33] Zhang Jiang. Quantum fisher information for states in exponential form. *Phys. Rev. A*, 89:032128, 2014.

[34] Jing Liu, Jie Chen, Xiao-Xing Jing, and Xiaoguang Wang. Quantum fisher information and symmetric logarithmic derivative via anticommutators. *J. Phys. A: Math. Theor.*, 49:275302, 2016.

[35] Katarzyna Macieszczak. Quantum fisher information: Variational principle and simple iterative algorithm for its efficient computation. *arXiv preprint arXiv:1312.1356*, 2013.

[36] Gabriela Wójtowicz, Susana F. Huelga, Marek M. Rams, and Martin B. Plenio. Quantum fisher information from tensor-network integration of the lyapunov equation. *Phys. Rev. A*, 112:052454, 2025.

[37] Víctor López-Pardo and Alexander Rothkopf. Optimal observables for (non-)equilibrium quantum metrology from the master equation. *arXiv preprint arXiv:2506.23600*, 2025.

[38] M. A. Manya, Andrei Tsypilnikov, and Fernando Iemini. Optimal observables for quantum-enhanced sensing and applications in a floquet time crystal sensor. *arXiv preprint arXiv:2606.26248*, 2026.

[39] Chang Shoukang, Marco G. Genoni, and Francesco Albarelli. Efficiently evaluating holevo, rld and sld cramér–rao bounds for multiparameter quantum estimation with gaussian states. *Commun. Phys.*, 9:126, 2026.

[40] Jia-Xuan Liu, Hai-Long Shi, Chunfeng Wu, and Sixia Yu. Quantum estimation with state symmetry-induced optimal measurements. *Nat. Commun.*, 17:7898, 2026.

[41] Chao Yin, Victor V. Albert, and Sisi Zhou. Metrologically optimal quantum states under noise. *Quantum*, 10:2050, 2026.

[42] Byeong-Yoon Go, Geunhee Gwak, Young-Do Yoon, Sungho Lee, Nicolas Treps, Jiyong Park, and Young-Sik Ra. Quantum metrology under coarse-grained measurement. *arXiv:2601.16106*, 2026.

[43] R. H. Bartels and G. W. Stewart. Algorithm 432: Solution of the matrix equation $ax + xb = c$. *Commun. ACM*, 15:820–826, 1972.

[44] Valeria Simoncini. Computational methods for linear matrix equations. *SIAM Rev.*, 58:377–441, 2016.

[45] Rolando D. Somma, Guang Hao Low, Dominic W. Berry, and Ryan Babbush. Quantum algorithm for linear matrix equations. *arXiv preprint arXiv:2508.02822*, 2025.

[46] Ewin Tang. A quantum-inspired classical algorithm for recommendation systems. *Proceedings of the 51st Annual ACM SIGACT Symposium on Theory of Computing*, pages 217–228, 2019.

[47] Nai-Hui Chia, Han-Hsuan Lin, and Chunhao Wang. Quantum-inspired sublinear classical algorithms for solving low-rank linear systems. *arXiv preprint arXiv:1811.04852*, 2018.

[48] Nai-Hui Chia, András Gilyén, Tongyang Li, Han-Hsuan Lin, Ewin Tang, and Chunhao Wang. Sampling-based sublinear low-rank matrix arithmetic framework for dequantizing quantum machine learning. *Proceedings of the 52nd Annual ACM SIGACT Symposium on Theory of Computing*, pages 387–400, 2020.

[49] András Gilyén, Zhao Song, and Ewin Tang. An improved quantum-inspired algorithm for linear regression. *Quantum*, 6:754, 2022.

[50] Dominik Šafránek. Discontinuities of the quantum fisher information and the bures metric. *Phys. Rev. A*, 95:052320, 2017.

[51] Luigi Seveso, Francesco Albarelli, Marco G. Genoni, and Matteo G. A. Paris. On the discontinuity of the quantum fisher information for quantum statistical models with parameter-dependent rank. *J. Phys. A: Math. Theor.*, 53:02LT01, 2020.

[52] A. T. Rezakhani, M. Hassani, and S. Alipour. Continuity of the quantum fisher information. *Phys. Rev. A*, 100:032317, 2019.

[53] Yating Ye and Xiao-Ming Lu. Quantum Cramér–Rao bound for quantum statistical models with parameter-dependent rank. *Phys. Rev. A*, 106:022429, 2022.

[54] Guang Hao Low and Isaac L. Chuang. Optimal hamiltonian simulation by quantum signal processing. *Phys. Rev. Lett.*, 118:010501, 2017.

[55] Guang Hao Low and Isaac L. Chuang. Hamiltonian simulation by qubitization. *Quantum*, 3:163, 2019.

[56] András Gilyén, Yuan Su, Guang Hao Low, and Nathan Wiebe. Quantum singular value transformation and beyond: Exponential improvements for quantum matrix arithmetics. In *Proceedings of the 51st Annual ACM SIGACT Symposium on Theory of Computing*, pages 193–204, 2019.

[57] Patrick Rall. Quantum algorithms for estimating physical quantities using block encodings. *Phys. Rev. A*, 102:022408, 2020.

[58] Marcello Benedetti, Ansis Rosmanis, and Matthias Rosenkranz. Probabilistic quantum algorithm for lyapunov equations and matrix inversion. *Phys. Rev. Applied*, 25:044040, 2026.

[59] Masahito Hayashi. *Quantum Information Theory: Mathematical Foundation*. Springer, Berlin, 2 edition, 2017.

[60] Zihao Gong and Boulat A. Bash. Two-stage quantum estimation and asymptotics of quantum-enhanced transmittance sensing. *Phys. Rev. A*, 113:052456, 2026.

[61] Joel Max. Quantizing for minimum distortion. *IRE Trans. Inf. Theory*, 6(1):7–12, 1960.

[62] Stuart P. Lloyd. Least squares quantization in PCM. *IEEE Trans. Inf. Theory*, 28(2):129–137, 1982.

[63] Robert M. Gray and David L. Neuhoff. Quantization. *IEEE Trans. Inf. Theory*, 44(6):2325–2383, 1998.

[64] Siegfried Graf and Harald Luschgy. *Foundations of Quantization for Probability Distributions*, volume 1730 of *Lecture Notes in Mathematics*. Springer, Berlin, 2000.

[65] Yating Liu and Gilles Pagès. Convergence rate of optimal quantization and application to the clustering performance of the empirical measure. *J. Mach. Learn. Res.*, 21(86):1–36, 2020.

[66] Philip F. Panter and William Dite. Quantization distortion in pulse-count modulation with nonuniform spacing of levels. *Proc. IRE*, 39(1):44–48, 1951.

[67] Paul L. Zador. Development and evaluation of procedures for quantizing multivariate distributions. Technical report, Stanford University, 1963.

[68] Paul L. Zador. Asymptotic quantization error of continuous signals and the quantization dimension. *IEEE Trans. Inf. Theory*, 28(2):139–149, 1982.

[69] Richard Bellman. A note on cluster analysis and dynamic programming. *Math. Biosci.*, 18:311–312, 1973.

[70] Haizhou Wang and Mingzhou Song. Ckmeans.1d.dp: Optimal k-means clustering in one dimension by dynamic programming. *R Journal*, 3(2):29–33, 2011.

[71] Jianqi Sheng. Task-dependent syndrome memory in quantum sensing and state recovery. *arXiv preprint arXiv:2608.02333*, 2026.

[72] Dhrumil Patel, Shi Jie Samuel Tan, Yiğit Subaşı, and Andrew T. Sornborger. Optimal coherent quantum phase estimation via tapering. *PRX Quantum*, 7:020302, 2026.

[73] Aram W. Harrow, Avinatan Hassidim, and Seth Lloyd. Quantum algorithm for linear systems of equations. *Phys. Rev. Lett.*, 103:150502, 2009.

[74] Andrew M. Childs, Robin Kothari, and Rolando D. Somma. Quantum algorithm for systems of linear equations with exponentially improved dependence on precision. *SIAM J. Comput.*, 46:1920–1950, 2017.

[75] Hugo Cable, Mile Gu, and Kavan Modi. Power of one bit of quantum information in quantum metrology. *Phys. Rev. A*, 93:040304, 2016.

[76] Mikko Möttönen, Juha J. Vartiainen, Ville Bergholm, and Martti M. Salomaa. Quantum circuits for general multiqubit gates. *Phys. Rev. Lett.*, 93:130502, 2004.

[77] Neil J. Ross and Peter Selinger. Optimal ancilla-free clifford+t approximation of z rotations. *Quantum Inf. Comput.*, 16:901–953, 2016.

[78] Jessica Lemieux, Guillaume Duclos-Cianci, David Sénéchal, and David Poulin. Resource estimate for quantum many-body ground-state preparation on a quantum computer. *Phys. Rev. A*, 103:052408, 2021.

[79] Florian Fröwis, Pavel Sekatski, and Wolfgang Dür. Detecting large quantum fisher information with finite measurement precision. *Phys. Rev. Lett.*, 116:090801, 2016.

[80] Ricard Puig, Pavel Sekatski, Paolo Andrea Erdman, Paolo Abiuso, John Calsamiglia, and Martí Perarnau-Llobet. From dynamical to steady-state many-body metrology: Precision limits and their attainability with two-body interactions. *PRX Quantum*, 6:030309, 2025.

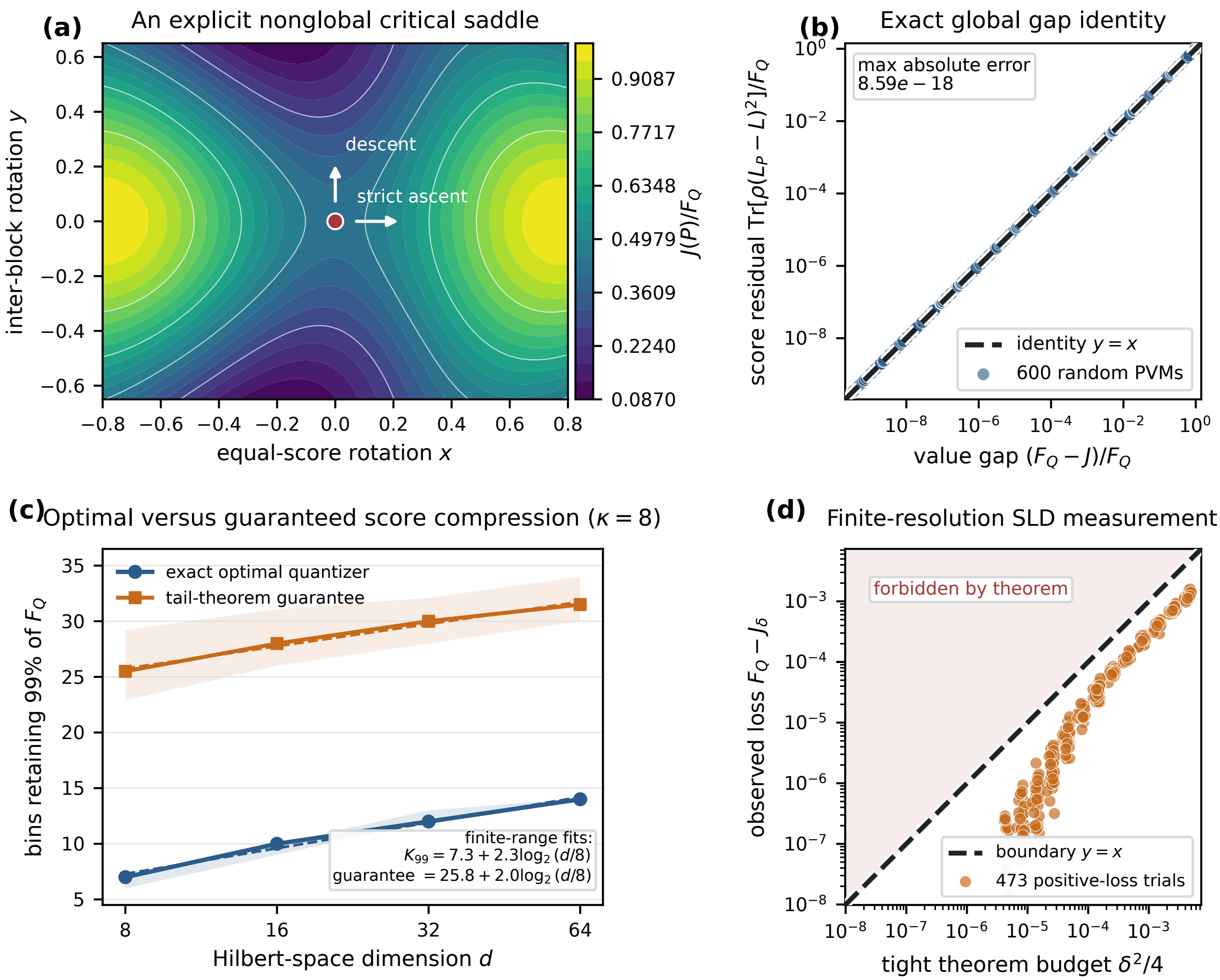

Figure 1: **Exact projective geometry and sharp score compression.** (a) A three-level Fisher landscape with a nonglobal critical saddle. The equal-score pair rotation supplied by Ref. [6] is a strict ascent direction. (b) Numerical closure of Eq. (48) for 600 PVMs in dimension 16; the dashed identity line is drawn above the points. (c) Exact optimal score bins retaining 99% of the QFI versus the constructive tail theorem. The finite-range median trend is logarithmic in the tested dimensions, without an asymptotic claim. (d) Direct test of Corollary 3.2; the half-plane above $y = x$ is forbidden by the sharp $\delta^2/4$ theorem.

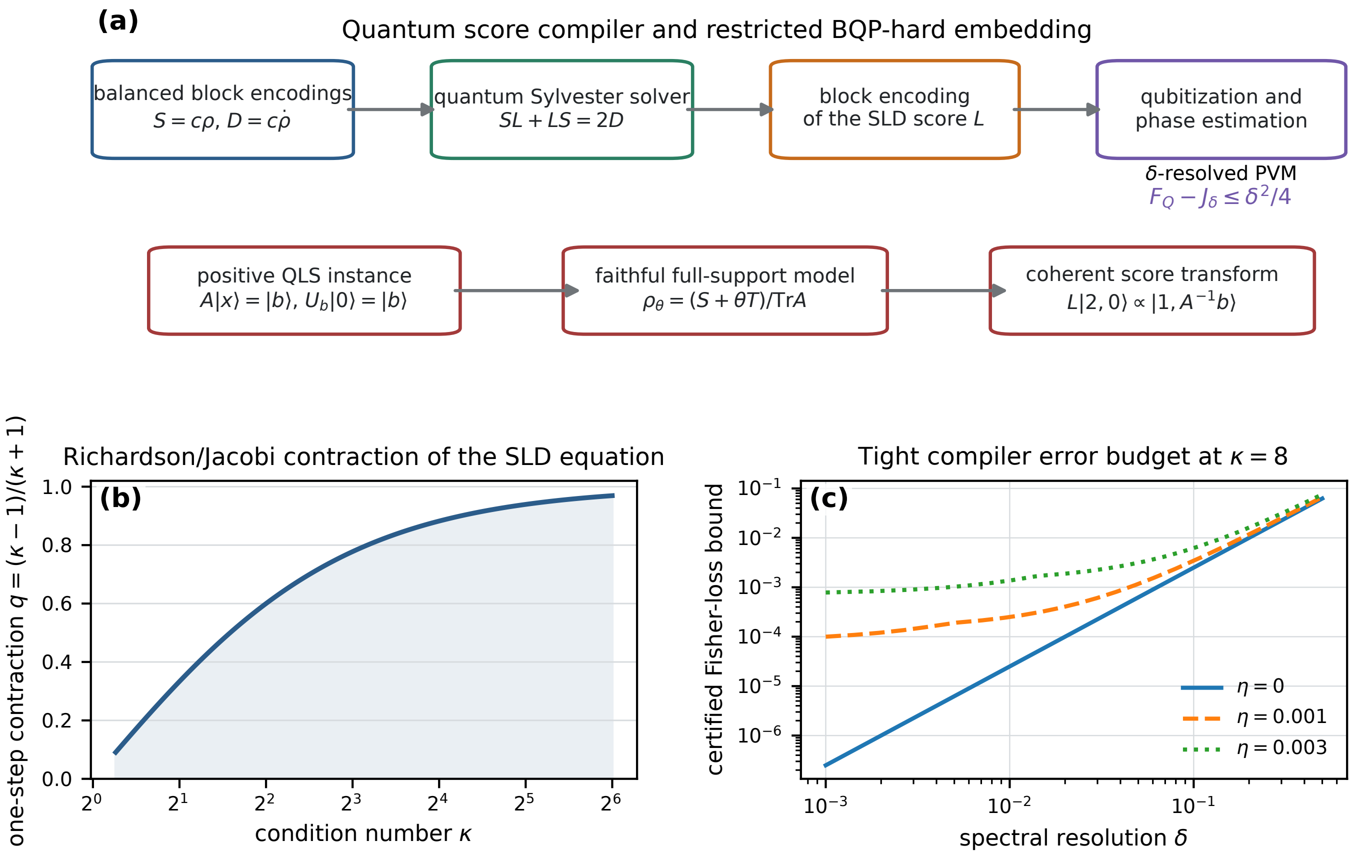

Figure 2: **Matrix approximation, operational interface, and the full-support hardness embedding.** (a) Top: balanced block encodings feed a quantum Sylvester solver; spectral processing produces an actual exhaustive label instrument whose score-intertwining defect is certified by Eq. (74). Bottom: the full-support reduction embeds positive QLS so that any delivered interface satisfying Eq. (82) maps a simple second-block input close to $A^{-1}|b\rangle$. (b) Exact one-step contraction of the classical Richardson/Jacobi baseline. It is a conditioning diagnostic. (c) Exact-$\widetilde{L}$ PVM Fisher-loss budget from Eq. (75) at $\kappa = 8$.

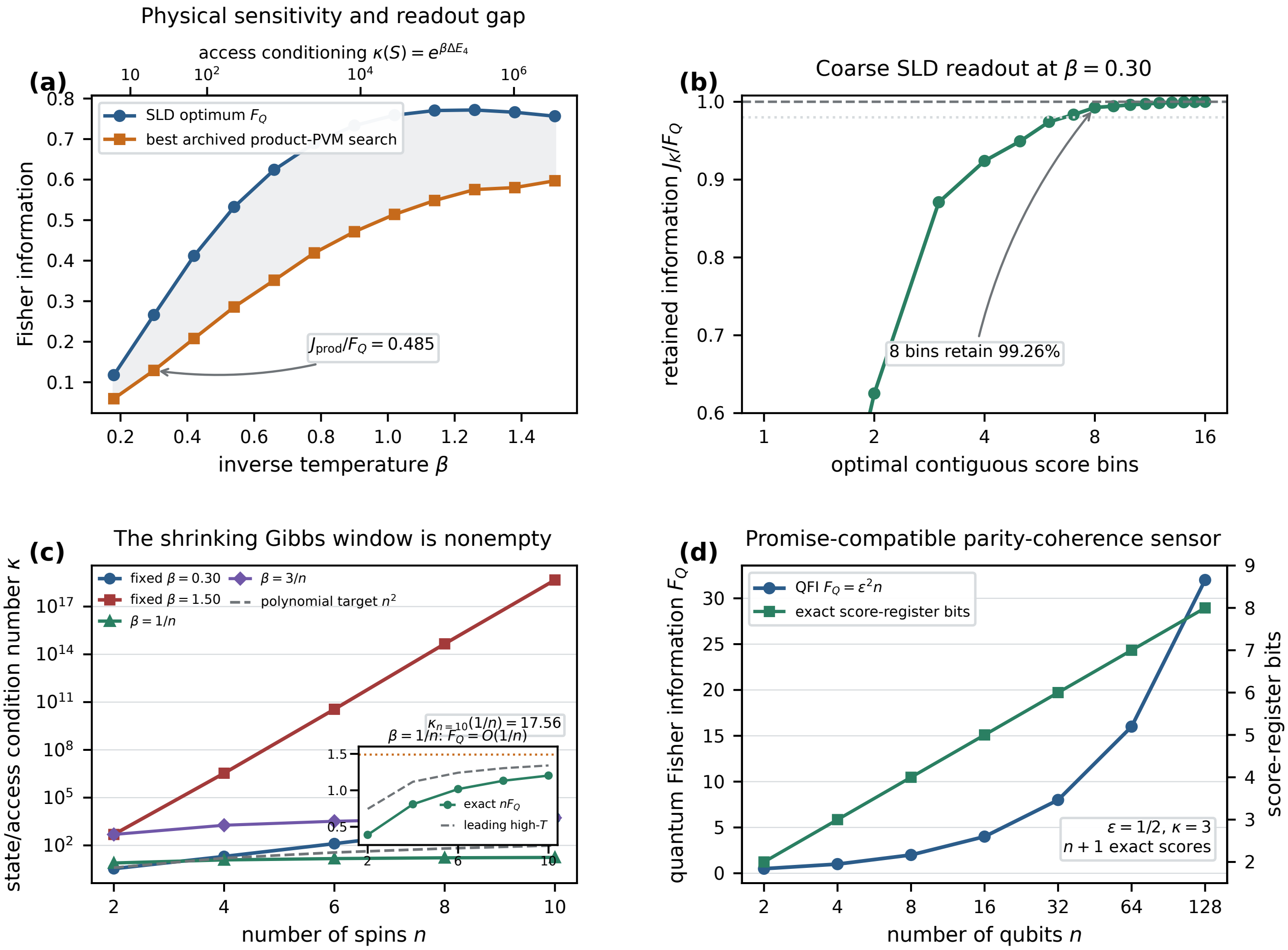

FIG. 3. Promise-compatible sensing, Gibbs access, and compressed readout. (a) QFI and the best product-PVM Fisher information found by the archived heuristic search for the frustrated four-spin sensor; the upper axis is the exact Gibbs condition number. (b) Exact optimal score quantization at $\beta = 0.30$: seven bins retain 98.34% and eight retain 99.26% of F_Q. (c) Fixed-temperature Gibbs conditioning grows exponentially with energy span, while $\beta = 1/n$ remains bounded over the tested sizes and has $F_Q = O(1/n)$ in the inset. (d) The parity-coherence family of Proposition 9.1: $F_Q = n/4$ at constant $\kappa = 3$, while the exact score label needs only $\lceil \log_2(n+1) \rceil$ bits.